Joule

CellPress
OPEN ACCESS

Article

Constraints on the Efficiency of Engineered Electromicrobial Production

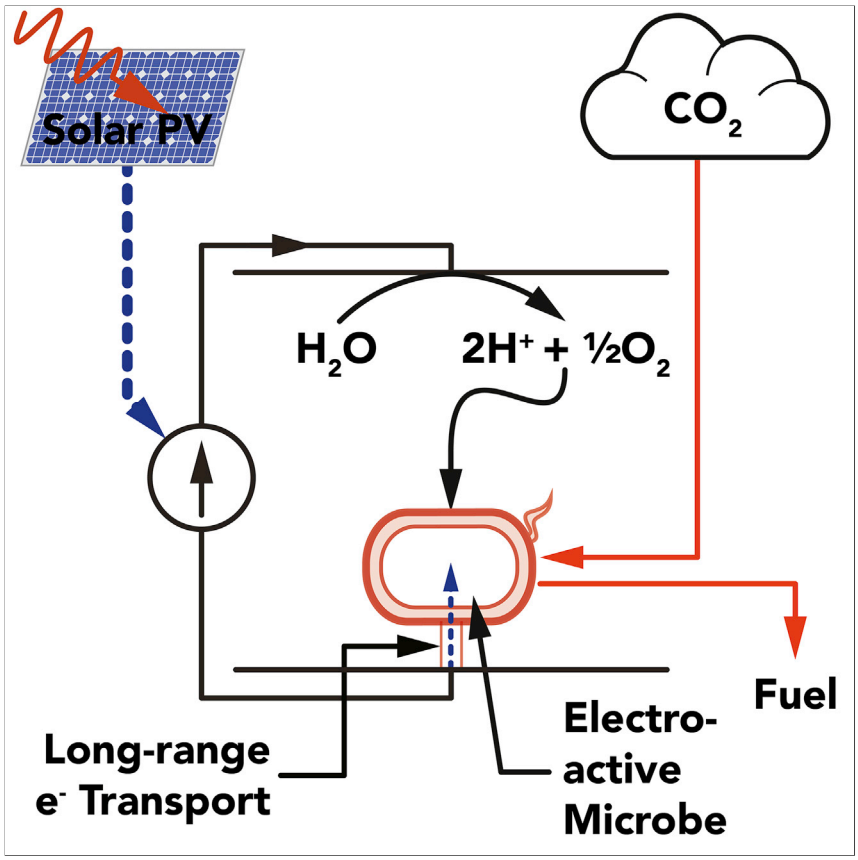

We have developed a theory that lets us calculate the efficiency of microbes that absorb electricity and store CO_2 as biofuels with greater efficiency than photosynthesis. We outline 10 development scenarios including re-engineering direct electron uptake microbes with high-efficiency CO_2 fixation; scaling up H_2-oxidizing microbe systems to store megawatts of electricity; engineering direct electron uptake microbes to make highly conductive artificial biofilms to enable high power density electricity storage; and engineering microbes that assimilate electrochemically reduced CO_2 with electron uptake.

Farshid Salimijazi, Jaehwan Kim, Alexa M. Schmitz, Richard Grenville, Andrew Bocarsly, Buz Barstow

bmb35@cornell.edu

HIGHLIGHTS

Predicts EMP electricity to biofuel conversion efficiency

Re-engineering *in vivo* CO_2 fixation can increase efficiency to ≈52%

EMP powered by H_2 oxidation is most efficient in ≥ 1 megawatt systems

EMP efficiency using electrochemically fixed CO_2 could exceed 50% with no O_2 sensitivity

Salimijazi et al., Joule 4, 2101–2130
October 14, 2020 © 2020 The Author(s).
Published by Elsevier Inc.
https://doi.org/10.1016/j.joule.2020.08.010

Joule

CellPress
OPEN ACCESS

Article

Constraints on the Efficiency of Engineered Electromicrobial Production

Farshid Salimijazi,[1] Jaehwan Kim,[2,4] Alexa M. Schmitz,[1] Richard Grenville,[3] Andrew Bocarsly,[2] and Buz Barstow[1,5,*]

SUMMARY

Electromicrobial production aims to combine electricity and microbial metabolism for solar and electrical energy storage. We have constructed molecule to reactor models of highly engineered electromicrobial production systems that use H_2 oxidation and direct electron transfer (DET). We predict electrical-to-biofuel conversion efficiency could rise to 52% with engineered *in vivo* CO_2 fixation. H_2 diffusion at ambient pressure requires areas 20 to 2,000 times the solar photovoltaic (PV) area supplying the system. Agitation can reduce this below the PV area, and the power needed is negligible when storing $\geq$1.1 megawatts. DET systems can be built with areas $\leq$ 15 times the PV area and have low energy losses even with natural conductive biofilms and can be even smaller if the conductivity could be raised to match conductive artificial polymers. Schemes that use electrochemical CO_2 reduction could achieve efficiencies of almost 50% with no complications of O_2 sensitivity.

INTRODUCTION

We are moving toward a world of plentiful renewable electricity.[1–3] However, to enable high penetration of renewables onto the grid, energy storage with a capacity thousands of times greater than today's will be essential.[4–7] On top of this, despite significant advances in electrified transportation, the need for hydrocarbons in many applications such as aviation could persist and even grow for decades to come.[3] Likewise, the need to sequester tens of gigatonnes of CO_2 per year will also continue to grow.[8,9] Electromicrobial production (EMP) technologies that combine biological and electronic components have the potential to use renewable electricity to power the capture and sequestration of atmospheric CO_2 and convert it into high-density, non-volatile infrastructure-compatible transportation fuels or energy storage polymers.[7,10–14]

At least two big classes of EMP technologies exist.[13,15] Given the rapid evolution of the field, these definitions can vary from author to author and may soon change,[15] but at the time of writing we believe they represent a widely acceptable classification. In the first class, electrons are either directly transferred from a cathode to microbial metabolism through a conductive extracellular matrix (ECM) (conductive ECM when it is synthesized chemically, or biofilm when it synthesized biologically, although we use these terms interchangeably for most of this article) to electrode-attached cells;[16] transported by complex biologically synthesized redox mediator molecules like flavins or phenazines to free-floating or cathode-attached cells;[10,17] or transported through biologically enhanced production of a simple redox mediator like H_2.[18–21] These modes of electron transport are often collectively referred

Context & Scale

The penetration of renewable electricity is increasing significantly making low-cost, large-scale energy storage essential. At the same time, the need for CO_2 sequestration and hydrocarbon fuels are likely to grow for decades to come. Photosynthesis gives a template for solar energy and CO_2 storage at enormous scale, but its inefficiency sets the stage for land competition.

We have developed a theory that lets us calculate the efficiency of microbes that absorb electricity and store CO_2 as biofuels with greater efficiency than photosynthesis. We outline 10 development scenarios including re-engineering direct electron uptake microbes with high-efficiency CO_2 fixation; scaling up H_2-oxidizing microbe systems to store megawatts of electricity; engineering direct electron uptake microbes to make highly conductive artificial biofilms to enable high power density electricity storage; and engineering microbes that assimilate electrochemically reduced CO_2 with electron uptake.

This is an open access article under the CC BY license (http://creativecommons.org/licenses/by/4.0/).

to as extracellular electron transfer (EET), but EET is sometimes informally (and technically incorrectly) used as a shorthand for direct electron transfer (DET). In this article we focus on DET and to avoid confusion will use the term DET, unless EET is a commonly used part of a name (e.g., the Mtr EET complex). This class of EMP technologies is often called microbial electrosynthesis (MES).[10,14,15]

A second class of EMP technologies use simple reduced soluble mediator compounds to shuttle electrons to microbial metabolism. To date, these mediators include H_2,[22–25] inorganic ions like ferrous ions,[26] ammonia,[27] and the simple organic molecule formate.[22,28–30] Additionally, carbon monoxide, formaldehyde, methane, methanol, phosphite, and reduced sulfur compounds (H_2S, $S_2O_3^{2-}$, $S_4O_6^{2-}$) could also be used as redox mediators,[7] but we are unaware of any demonstrations to date. These electron shuttles can either be directly electrochemically reduced or produced by reaction of electrochemically reduced H_2 with CO_2 or another inorganic compound, or both. These technologies are sometimes called secondary microbial electrochemical technologies (MET).[15] Electron transfer by H_2 sometimes falls into the MES category when H_2 production is enhanced by presence of microbes on the cathode.[14,18] On the other hand, when the electrochemical production of H_2 has no biological component, it can fall into the secondary MET category.

EMP technologies have made considerable advances over the past decade. Numerous studies have demonstrated acetic and butyric acid production by MES[14,31–52] with faradic efficiencies well over 80%[31,32,34] if not 90%.[33,38,42] Over the same time, indirect electron transfer via H_2 has led to some of the most substantial advances in MES systems.[18–21] Meanwhile, one of the most prominent demonstrations of EMP to date, the Bionic Leaf,[23,24] is capable of converting solar power to the biofuel isopropanol through a H_2 mediator at efficiencies exceeding the theoretical maximum of C_3 and C_4 photosynthesis.[53,54] Meanwhile, Haas et al. demonstrated electrochemical conversion of CO_2 and H_2O to syngas followed by microbial fermentation to butanol and hexanol with nearly 100% faradic efficiency.[25] If coupled to some of the most efficient Si or GaAs solar photovoltaics (PVs),[55] the Bionic Leaf could even outperform cyanobacterial photosynthesis, the most efficient form found in nature.[56] Yishai et al.[28] and Tashiro et al.[57] have both demonstrated formate assimilation by engineered *E. coli*. Furthermore Kim et al. have demonstrated the growth of engineered *E. coli* on formate, while Gleizer et al. have demonstrated the growth of *E. coli* on CO_2 and formate.[29]

Despite all of this progress, the problem of electron supply needs to be met for EMP to achieve its promise. As the energy storage cost of photosynthesis is ultra low,[58,59] any system that aims to supplant it will need to dramatically exceed its efficiency, its convenience, and preferably both. Despite the many advantages of formate, including high solubility and high faradic efficiency of electrochemical production,[13] formate is too lightly reduced for many applications (formate only carries 2 electrons per carbon). For example, in order to produce a fuel alcohol molecule (6 electrons per carbon) from CO_2, an organism that relies only on formate for electron and carbon supply will need to re-release approximately 2/3rds of the initially reduced CO_2 back into the atmosphere. Likewise, despite the advantages of H_2 as a mediator,[18,23–25] its low solubility in water means that its use is likely to pose energetic, geometric, and safety challenges on scale up.[60–62] DET systems solve many of the issues associated with H_2, but the incompatibility of many microbes capable of DET with high osmotic strength electrolytes leads to high internal electrochemical cell resistances and correspondingly low overall energy conversion efficiencies.[14]

[1]Department of Biological and Environmental Engineering, Cornell University, Ithaca, NY 14853, USA

[2]Department of Chemistry, Princeton University, Princeton, NJ 08544, USA

[3]Philadelphia Mixing Solutions Ltd., Palmyra, PA 17078, USA

[4]Present address: Department of Chemistry and Chemical Biology, Cornell University, Ithaca, NY 14853, USA

[5]Lead Contact

*Correspondence: bmb35@cornell.edu

https://doi.org/10.1016/j.joule.2020.08.010

Furthermore, although MES systems are able to direct a very high percentage of metabolic flux toward acetate production, they are unable to do the same for other bio-products like biofuels.[14] Finally, until recently, considerable debate has raged about the nature of DET from a cathode across a conductive biofilm to the cell surface, and from the cell surface into the reductant pool in the cell.[14]

To fully achieve the potential of EMP, innovations in reactor design, process design, and perhaps most importantly genetic engineering of the EMP host will be required.[14,63] What will this organism look like? We see at least four important characteristics. First, the organism will receive electrons through a mechanism that enables the lowest cost, most reliable reactor design, and most efficient process. Second, the organism will be highly tolerant of the electrochemical environment that enables the highest energy conversion efficiency. Third, the organism will have minimal matter and energy requirements for cellular maintenance. Finally, it will transfer almost all carbon entering the system to a single product with high energy efficiency. Engineering this organism will almost certainly be a grand challenge in synthetic biology. This raises two important questions: first, is the payoff for all the genetic engineering worth the effort? Second, is there an easily understood standard for success that synthetic biologists can compare their efforts with? While no one metric can capture every aspect of an organism's suitability, we believe that energy conversion efficiency is the one metric that most closely relates to the success of EMP in the real world. Furthermore, we believe that by calculating a simple upper limit target based upon simple physical considerations, we can spur synthetic biologists toward progress in the field, much in the same way that theoretical predictions of solar photovoltaic conversion efficiencies[64,65] have spurred decades of solar PV efficiency improvements. For example, the energy conversion efficiency of silicon solar cells now stands at 26.7%,[55] close to the Shockley-Quiesser limit of 32.9%.[64,66]

To date, while there has been considerable work on modeling mechanisms for electron transfer in microbial electrosynthesis,[17,67] modeling EMP,[68,69] and compiling estimates of EMP efficiency through big data-driven back of the envelope calculations,[13] very little work has focused on systematically exploring the intra- and extracellular constraints on the overall energy conversion efficiency of electricity and CO_2 to bio-products by engineered EMP systems.

Here, we present an analytical thermodynamic and kinetic framework for making apples-to-apples comparisons of the theoretical maximum efficiencies of highly engineered EMP systems. For simplicity, in this article, we consider four model EMP systems. While we cannot cover all possible EMP systems (systems that convert electricity and CO_2 to more complex molecules like biofuels), we believe this set is the most illustrative example of all systems and can be readily adapted to any system. Each of these systems transform CO_2 to the biofuels isopropanol[70] or butanol.[22,59,71] We consider a pair of systems that use *in vivo* CO_2 fixation Figure 1A. In the first system, electrons are transferred by electrochemically produced H_2 representative of systems in Torella et al.,[23] Liu et al.,[24] and Haas et al.[25] (Figure 1C). In the second system, electrons are directly transferred through a conductive ECM to a CO_2-fixing microbe representative of engineered microbial electrosynthesis systems[72] (Figure 1D).

We then consider a pair of systems in which CO_2 is first electrochemically reduced to a short-chain hydrocarbon such as formate or formic acid[73–75] (Figure 1B). In the third system electrons are delivered through electrochemically reduced H_2 for further

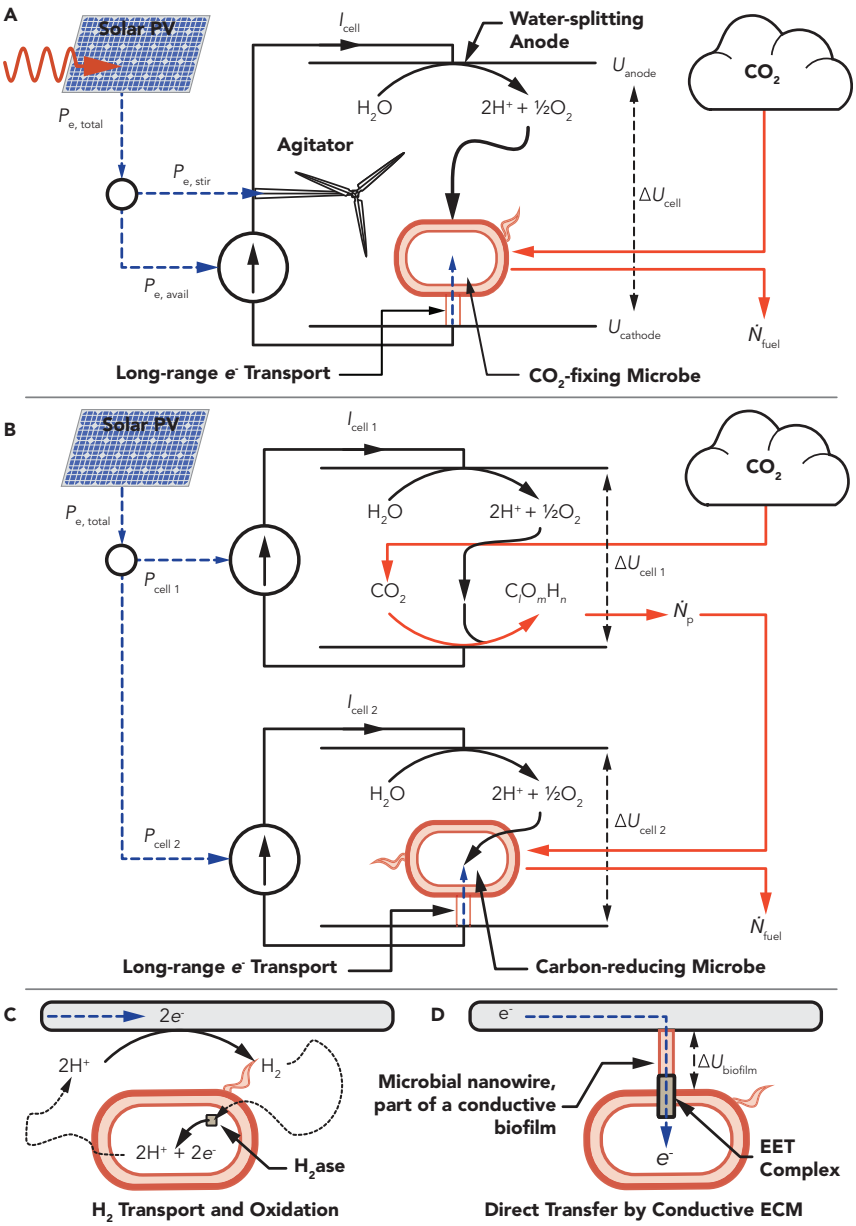

Figure 1. Overview of Representative Electromicrobial Production Technologies

(A) A microbe absorbs electrical power, $P_{e,\ avail}$, through H_2-oxidation or directly through a conductive extracellular matrix (ECM) to power CO_2-fixation and biofuel production at a rate $\dot{N}_{fuel}$. The total electrical power is used to drive a current, I_{cell}, across a whole-cell voltage, ΔU_{cell}, and can also be used to power an agitator.

(B) The electrical power is split between two electrochemical cells. In the first CO_2 is reduced to a short chain hydrocarbon like formic acid at a rate $\dot{N}_p$. The primary fixation product is then concatenated in the second cell by a H_2-oxidizing or electroactive microbe.

(C and D) Electrons are transported to metabolism by either (C) diffusion or stirring of H_2 and oxidation by a hydrogenase (H_2ase) enzyme, or (D) directly across a conductive ECM and transfer into an electroactive cell by a membrane-spanning EET complex. A voltage $\Delta U_{biofilm}$ is required to drive current across the ECM.

bioelectrochemical reduction of formate to a biofuel[22] (Figure 1C). Finally, we consider a system where electrons are transferred to a microbial host directly by a conductive ECM for further reduction of formate (Figure 1D).

It is important to stress that our results do not apply to any specific naturally occurring or lightly engineered system (for instance, a naturally occurring microbe with a few additional genes added to synthesize a biofuel) but to a reactor-microbe system that is highly engineered, both at the reactor and genetic level, to operate at the limit of its potential. This analysis lets us calculate the maximum theoretical efficiency of each EMP system and gives a roadmap for how to achieve it.

RESULTS AND DISCUSSION

A complete list of symbols used in this article is included in Table S1.

We define the electrical energy conversion efficiency as the rate of energy storage molecule production, $\dot{N}_{fuel}$, multiplied by the energy content per molecule, E_{fuel}, relative to the total electrical power input:

$$\eta_{EF} = \dot{N}_{fuel} E_{fuel} \Big/ P_{e,\,total}. \qquad \text{(Equation 1)}$$

H_2-Mediated EMP is Already Optimized but Can Be Improved by Swapping Out CO_2 Fixation

Estimating the efficiency of *in vivo* CO_2 fixation (Figure 1A) comes down to estimating $\dot{N}_{fuel}$ as a function of the electrical power available for electrochemistry, $P_{e,\,avail}$; the voltage across the electrochemical cell, ΔU_{cell}; and the number of electrons needed to generate the NAD(P)H, Ferredoxin (Fd), and ATP for synthesis of a single fuel molecule from CO_2, ν_{ef} (e = elementary charge) (Supplemental Experimental Procedure 1):

$$\dot{N}_{fuel} \leq P_{e,\,avail} \Big/ (e\nu_{ef}\Delta U_{cell}) \qquad \text{(Equation 2)}$$

Therefore, the overall electrical to fuel efficiency for an *in vivo* CO_2-fixation scheme:

$$\eta_{EF} \leq E_{fuel}/(e\nu_{ef}\Delta U_{cell}) \qquad \text{(Equation 3)}$$

ν_{ef} can be estimated from molecular models of electron uptake either by H_2 oxidation in this case or by direct electron uptake. A schematic of the *Ralstonia eutropha* H_2-oxidation machinery (used by Li et al.,[22] Torella et al.,[23] and Liu et al.[24]) is shown in Figure 2A. The low redox potential of H_2 (U_{H_2}) enables direct reduction of NAD^+ by the cytosolic nickel-iron soluble hydrogenase (SH) (*R. eutropha* uses NADH rather than NADPH for CO_2 fixation).[62,76] While the *R. eutropha* genome does not code for any Fd-reducing di-iron hydrogenases, these could be readily added to it.[77–79] Thus, the microbe simply has to oxidize a number of H_2 molecules equal to the sum of NADH and Fd that it needs to synthesize a fuel molecule (the number of electrons needed is just double the number of H_2). In this work, we consider only one CO_2-fixation cycle, the dicarboxylate/4-hydroxybutyrate (4HB) cycle,[80] that requires Fd.

We make the assumption that the cell is pre-grown and is simply mediating electron uptake by H_2 oxidation or DET, the fixation of CO_2 or further reduction of formate, and the synthesis of biofuels. We further make the assumption that reactants (CO_2 and electricity) are constantly input into the system and that product (biofuel) is continuously removed. This does not correspond exactly to any natural state or bacterial growth stage (e.g., exponential phase where naturally occurring microbes are most active) but is closer to the state of differentiated red blood cells that simply act as a "bag of enzymes" for O_2 transport and perform minimal cellular maintenance for

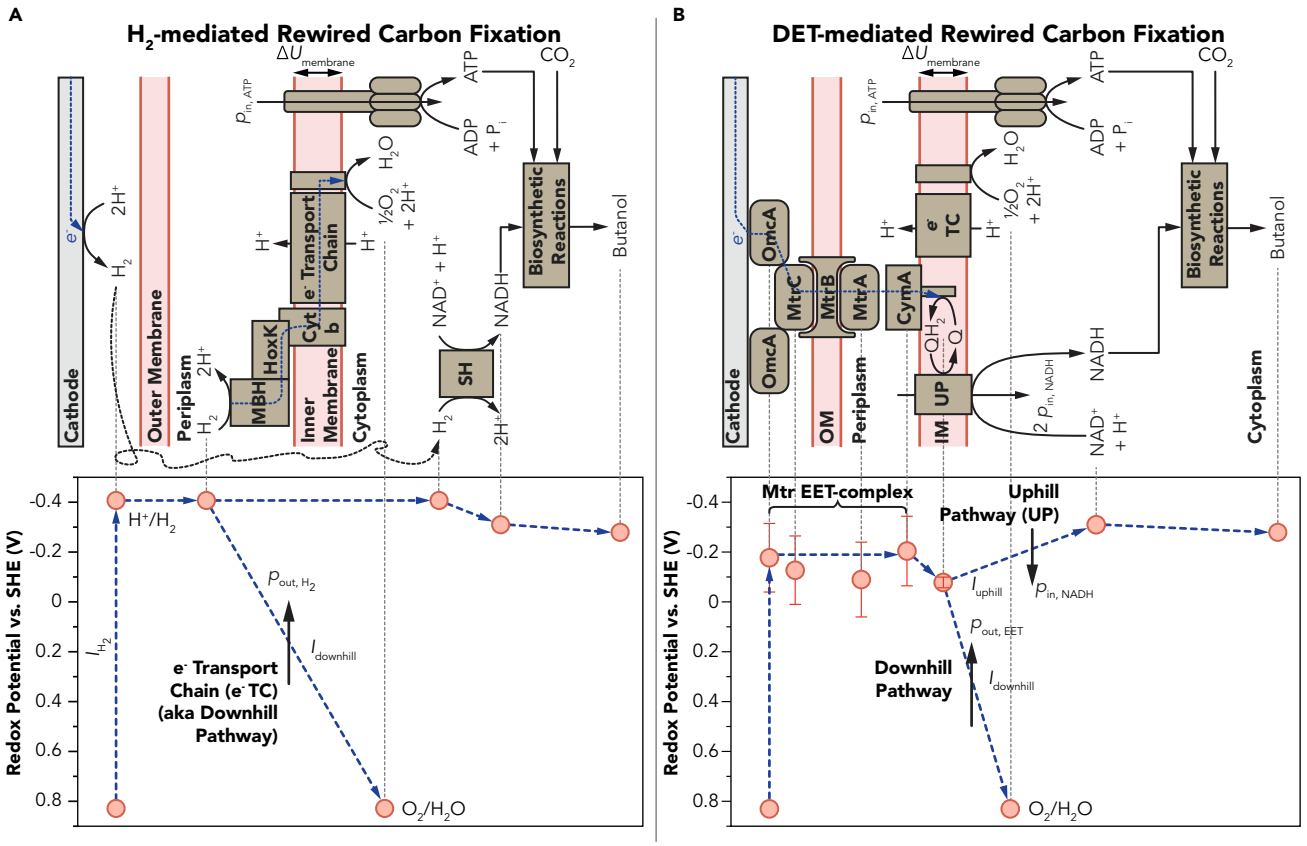

Figure 2. Energy Landscapes for Electromicrobial Production

(A) In H_2-mediated EMP, the incoming H_2 current is used to directly reduce NAD(P)H or ferredoxin (not shown) or is diverted into the conventional electron transport chain for ATP synthesis. For each electron sent downhill to reduce O_2 and H^+ to H_2O, $p_{out,H2}$ are pumped across the inner membrane. To regenerate an ATP molecule, $p_{in,ATP}$ protons are released through the ATP synthase.

(B) In DET-mediated EMP the incoming current is split between the uphill and downhill pathways. For each electron sent downhill, $p_{out,EET}$ protons are pumped across the inner membrane. For each electron sent uphill in energy to reduce NAD^+ to NADH, $p_{in,NADH}$ are pumped into the cytosol. Midpoint redox potentials for the Mtr EET complex components are from Firer-Sherwood et al.[113]

their lifetime of ≈ 80 to 120 days[81] (in our case, the cell is more like a box of enzymes and metalloproteins, some of which are localized on the inner and outer membranes). We make the further assumption that the inner membrane proton gradient is already established and that a negligible amount of power is expended for cellular maintenance. Thus, our efficiency calculations represent peak, upper limit values, and are only likely to be approached when peak cell density has been achieved, and the cell is performing maintenance. We assume that excess energy is dissipated as heat and that the system operates in an infinite heat sink.

Is it reasonable to assume that cellular growth and maintenance energy requirements are negligible? We estimate, based upon modeling by Kliphuis et al.,[82] a cellular maintenance energy requirement of $\approx 1 \times 10^{-14}$ W cell^{-1} (with the snote-growth_-maintenance_energy.py program that is part of the REWIREDCARBON package and in Supplemental Experimental Procedure 12). In contrast, the electrical power delivered to each cell is $\approx 1 \times 10^{-11}$ W cell^{-1}. This means the maintenance energy is only about $\approx 10^{-4}$ of the power available to the cell (this ratio is rounded after calculation with the unrounded maintenance and input power numbers), far less than the precision quoted for efficiencies in this article. This power requirement would need to increase by ≈ 100-fold to noticeably change reported efficiency predictions.

Likewise, biomass growth energy requirements could also be negligible compared with the amount of electrical energy that a maximally active EMP cell needs to convert to chemical energy over its lifespan. We calculate (with snote-growth_maintenance_energy.py and in Supplemental Experimental Procedure 12) that ≈4 g of dry cell mass is needed to process the electrical power from a 1 m^2 solar panel (330 W) and that $\approx 2\times10^4$ J of energy is needed to produce this biomass. This energy is delivered to the cells approximately every 1 min. This means that the EMP biomass only needs to survive for a few hours in order for the energy needed to grow it to become negligible.

ATP is generated by injection of electrons from H_2 oxidation by the membrane-bound hydrogenase (MBH) into the inner membrane electron transport chain;[62,76] quantized energy transduction by proton pumping against the transmembrane voltage, $\Delta U_{membrane}$; reduction of a terminal electron acceptor at a redox potential $U_{Acceptor}$; and further quantized energy transduction by proton release through the ATP synthase and ATP regeneration. In all calculations in this article, we assume the use of O_2 as a terminal electron acceptor at the end of the electron transport chain (Figure 2).

Therefore, the number of electrons needed to synthesize a single fuel molecule through H_2 oxidation is (a full derivation is included in Supplemental Experimental Procedure 2) ($\nu_{f,NADH}$, $\nu_{f,Fd}$, and $\nu_{f,ATP}$ are the number of NAD(P)H, Fd, and ATP needed for synthesis of a single fuel molecule, respectively):

$$\nu_{ef,\,H_2} = 2\,\nu_{f,\,NADH} + 2\,\nu_{f,\,Fd} + \nu_{f,\,ATP}\frac{\mathrm{ceil}\left(\Delta G_{ATP/ADP}/e\,\Delta U_{membrane}\right)}{\mathrm{floor}\left(\left(U_{H_2} - U_{Acceptor}\right)/\Delta U_{membrane}\right)}. \quad \text{(Equation 4)}$$

These equations are numerically solved with the REWIREDCARBON package using estimates for the NAD(P)H, ATP and Fd requirements for isopropanol and 1-butanol synthesis (Figure S3) from CO_2 fixed by the known natural CO_2-fixation cycles and the synthetic CETCH cycle[83] in Table S2. A workflow for the electrosynthesis efficiency calculation algorithm used in the REWIREDCARBON package is shown in Figure 3, and a set of parameters for four reference models are shown in Table 1.

The biggest source of uncertainty in the efficiency estimate is the transmembrane voltage ($\Delta U_{membrane}$). At the time of writing, we are unaware of any direct measurement of $\Delta U_{membrane}$ in *R. eutropha* or the electroactive microbe *Shewanella oneidensis*. Therefore, in Figure 4 we present a range of efficiency estimates for $\Delta U_{membrane}$=80 mV (BioNumber, ID (BNID) 104082[84]) to 270 mV (BNID 107135), with a central value of 140 mV (BNIDs 109774, 103386, and 109775). Counterintuitively, the efficiency of H_2-mediated EMP trends downward, moving from plateau to plateau, with increasing transmembrane voltage (Figure S1). While the amount of energy stored per proton is lower at lower $\Delta U_{membrane}$, energy quantization losses are also reduced. The transmembrane voltage is a function of the difference in ion concentrations between the cytoplasmic and periplasmic side of the inner membrane and can be modulated genetically by changing the expression levels of ion transporters in the inner membrane.[85]

This framework estimates the electron requirement for isopropanol and butanol synthesis by the Bionic Leaf (H_2-EMP using the Calvin cycle (CBB) for *in vivo* CO_2 fixation) to be $25^{+0.5}_{-3.5}$ and $31^{+0.5}_{-3.5}$, respectively. The maximum electricity to isopropanol

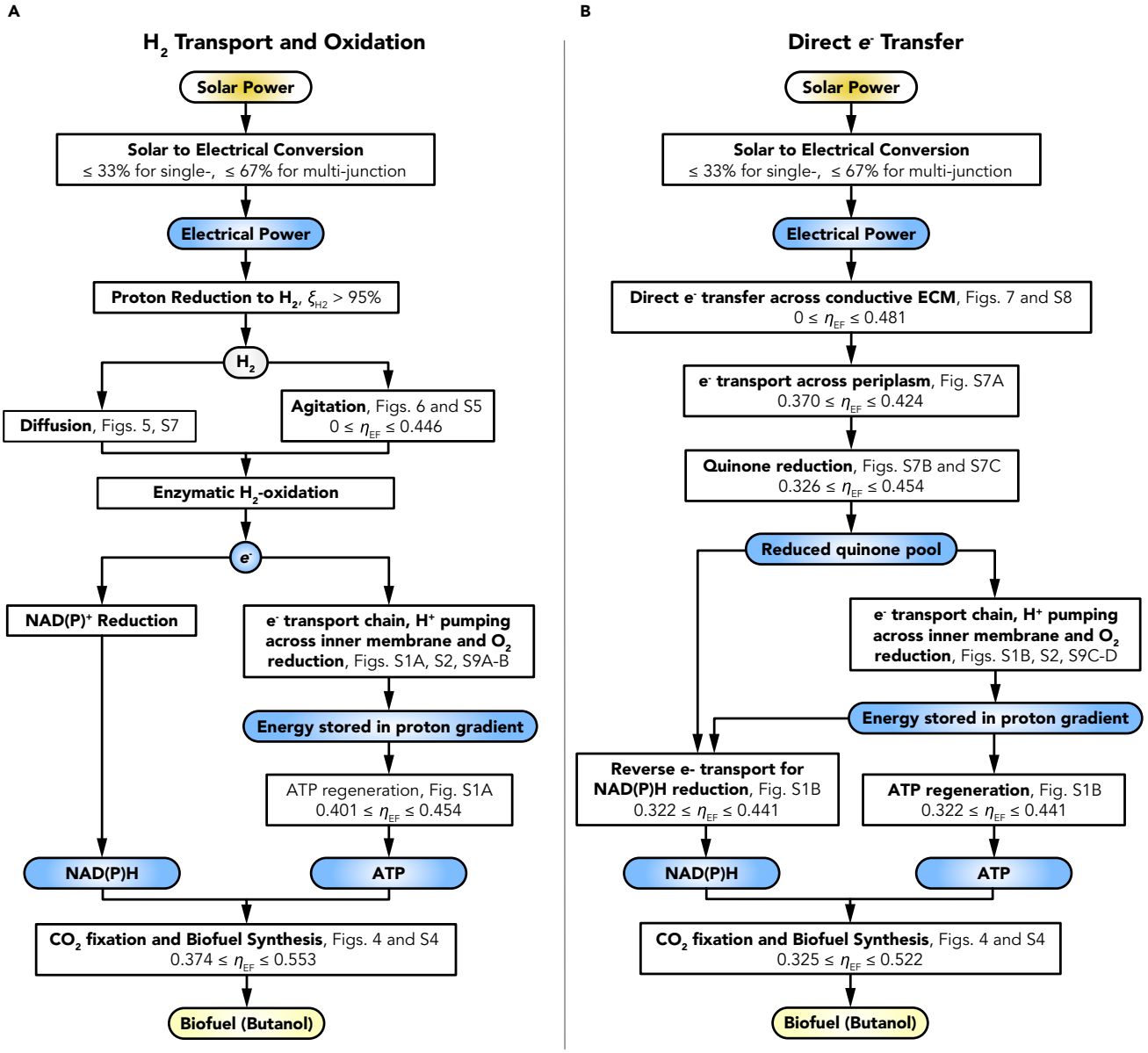

Figure 3. Key Steps of Electromicrobial Production Efficiency Calculation Algorithm

(A) Steps in calculation of efficiency of H_2-mediated EMP along with their ability to modulate electrical to fuel efficiency (η_{EF}) of the H_2-EMP reference model (model 1 in Table 1; bar D in Figure 4, η_{EF} = 0.446).

(B) Steps in calculation of efficiency of DET-mediated EMP along with their effect on electrical to fuel efficiency of DET-EMP (model 2 in Table 1, bar L in Figure 4, η_{EF} = 0.421).

conversion efficiency of the Bionic Leaf (ΔU_{cell}=2[24]) is estimated to be $41.6^{+0.8}_{-5.1}$%(Figure 4C). This result just exceeds the maximum reported electrical to isopropanol efficiency of 39±2%.[24] This match suggests that CO_2-fixation and biofuel synthesis in *R. eutropha* are already highly optimized.

As a sanity check, we computed the number of protons that need to be pumped back into the cytosol through the ATP synthase to regenerate a single ATP molecule as a function of transmembrane voltage, $\Delta U_{membrane}$ (Figure S2). For 140≤ $\Delta U_{membrane}$<187 mV, four protons need to be pumped to regenerate one ATP, equal

Table 1. Input Parameters for Models of Four Representative Electromicrobial Production Systems

Parameter	Symbol	1. H_2 oxidation	2. Direct e^- Transfer	3. H_2 oxidation with Formate	4. Direct e^- Transfer with Formate
Electrochemical Cell Parameters					
Input solar power (W)	P_γ	1,000 (Figure 6)	1,000	1,000	1,000
Bar label In Figure 4		D	L	T	S
Total available electrical power (W)	$P_{input,\ total}$	330 (Figure 6)	330	330	330
CO_2-fixation method		enzymatic		electrochemical	
Electrode to microbe mediator		H_2	direct	H_2	direct
Cell 1 cathode std. potential (V)	$U_{cell\ 1,\ cathode,\ 0}$	N/A		0.82[23]	
Cell 1 cathode bias voltage (V)	$U_{cell\ 1,\ cathode,\ bias}$	N/A		0.47[24]	
Cell 1 anode std. potential (V)	$U_{cell\ 1,\ anode,\ 0}$	N/A		−0.43[28,167]	
Cell 1 anode bias voltage (V)	$U_{cell\ 1,\ anode,\ bias}$	N/A		1.3[74]	
Cell 1 voltage (V)	$^{\Delta}U_{cell\ 1}$	N/A		3.02	
Cell 1 Faradaic efficiency	ξ_{11}	N/A		0.8 [168]	
Carbons per primary fixation product	ν_{Cp}	N/A		1	
e− per primary fixation product	N_{ep}	N/A		2	
Cell 2 (Bio-cell) anode std. potential (V)	$U_{cell\ 2,}$ anode, 0	−0.41[23]	−0.1[102,113]	−0.41	−0.1
Bio-cell anode bias voltage (V)	$U_{cell\ 2,\ anode,\ bias}$	0.3[24]	0.2[72]	0.3	0.2
Bio-cell cathode std. potential (V)	$U_{cell\ 2,\ cathode,\ 0}$	0.82			
Bio-cell cathode bias voltage (V)	$U_{cell\ 2,\ cathode,\ bias}$	0.47			
Bio-cell voltage (V)	$\Delta U_{cell\ 2}$	2[24]	1.59	2	1.59
Bio-cell Faradaic efficiency	ξ_{12}	1.0			
Cellular Electron Transport Parameters					
Membrane potential difference (mV)	$^{\Delta U}$membrane	140 (Figure S1)		140	
Terminal e^- acceptor potential (V)	^{U}Acceptor	0.82			
Quinone potential (V)	U_Q	-0.0885 (Figure S6)		−0.0885[102]	
Mtr EET complex potential (V)	^{U}Mtr	N/A	−0.1 (Figure S6)	N/A	−0.1
No. protons pumped per e^-	^{P}out	unlimited (Figure S9)		Unlimited	
CO_2 Fixation and Biofuel Synthesis Parameters					
Biofuel produced		Butanol			
No. ATPs for fuel synthesis	$^{\nu}$f, ATP	14 (Figure S4)		8	
No. NAD(P)H for Fuel	$^{\nu}$f, NADH	12 (Figure S4)		6	
No. ferredoxin for Fuel	$^{\nu}$f, Fd	0 (Figure S4)		0	
No. CO_2 fixed per fuel	$^{\nu}$Cf fix	6 (Figure 4)		N/A	
No. carbon atoms per fuel	$^{\nu}$Cf	4 (Figure 4)			
No. e^- per fuel	$^{\nu}$ef	24 (Figure 4)			
Energy density of fuel (J molecule^{-1})	^{E}fuel	4.43×10^{-18} (Figure 4)			
No. primary fixation product per fuel	ν_P	N/A	N/A	6	6
Scale-Up Parameters					
H_2 partial pressure (Pa) in bio-cell	PH2	(Figure 5)	N/A	–	N/A
Cell density (cells m^{-3})	^{n}cells	(Figures 5 and 6)	N/A	–	N/A
Cell length (μm)	^{l}cell	3.9			
Cell diameter (μm)	^{d}cell	1.3			
CO_2-fixing enzyme rate (s^{-1})	^{r}fix	12		N/A	
CO_2-fixing enzymes per cell	$^{\nu}$fix	10^6		N/A	

(*Continued on next page*)

Table 1. *Continued*

Parameter	Symbol	1. H_2 oxidation	2. Direct e^- Transfer	3. H_2 oxidation with Formate	4. Direct e^- Transfer with Formate
ECM thickness (μm)	^{h}biofilm	N/A	(Figure 7)	N/A	–
ECM layer fill factor	$f$layer	N/A	0.25	N/A	0.25
ECM layer height (μm)	^{h}layer	N/A	2.6	N/A	2.6
ECM resistivity (Ω cm)	$^\rho$biofilm	N/A	(Figure 7)	N/A	–
Electrical to fuel efficiency	$^\eta$EF	0.446	0.421	0.444	0.431

ECM, extracellular matrix; EET, extracellular electron transfer. A full list of symbols and corresponding computer variables in the REWIREDCARBON package is shown in Table S1. References for metabolic pathway parameters are shown in Table S2, while references for electrochemical parameters can be found next to the corresponding variable in this table. A reference to a figure showing the effect of varying a model parameter is shown in parentheses next to the parameter value. If only a figure reference is shown, then this parameter is not used in the reference case calculation.

to the number commonly accepted for ATP regeneration in the cyanobacterium *Synechocystis* 6803.[86] For $187 \leq \Delta U_{membrane} < 280$ mV, three protons need to be pumped, equal to the commonly accepted number for ATP regeneration in *E. coli*.[87] We also computed the effect of limiting the number of protons that could be pumped out of the cytosol for each electron sent downhill in energy to O_2 reduction in Figure S9.

How high could the efficiency go? Switching the product to butanol affords an improvement in H_2-EMP efficiency to $44.6^{+0.7}_{-4.5}$% and a significant improvement in ease of product recovery (bar D Figure 4D; model 1 in Table 1). If the anode and cathode bias voltages (the additional voltage supplied by a potentiostat beyond the thermodynamic minimum required to catalyze the anode and cathode reactions) could be reduced to zero, the efficiency of H_2-EMP electrical to 1-butanol efficiency could rise as high as $72.5^{+1.1}_{-7.4}$% (bar I). However, given the already-low cobalt phosphate electrode overpotentials[88] in the Bionic Leaf, raising the efficiency by this route might be impractical.

Could the efficiency of EMP be increased by altering just the biological part of the system? Following intuition, electrical to fuel efficiency increases with decreasing NAD(P)H, ATP and Fd requirements for CO_2 to biofuel conversion (Figures S4A–S4D). The efficiencies of the six known naturally occurring carbon fixation pathways and the synthetic CETCH pathway are shown in Figure 4. The CETCH[83] cycle matches the efficiency of CBB (bar E), while the naturally occurring CO_2-fixation cycles 3HP-4HB (bar F), rTCA (bar G) and WL (bar H) all perform better than the Calvin cycle, raising the electrical to fuel efficiency as high as $55.3^{+0.1}_{-1.1}$%. ATP, NAD(P)H, Fd, and carbon requirements for all metabolic pathways considered in this article are shown in Table S2. Marshall et al. recently demonstrated high-performance EMP by an acetogenic microbial community in which the primary CO_2-fixation method was likely the Wood-Ljungdahl pathway.[89] We calculate the upper limit efficiency of acetogenesis with the Wood-Ljungdahl pathway to be $87.2^{+1.0}_{-2.6}$%, when anode and cathode overpotentials are set to zero (bar R).

It is important to note that the O_2-sensitivity of both the rTCA cycle and the Wood-Ljungdahl pathway means that it is not yet, and may never be, possible to use O_2 as an electron acceptor while simultaneously operating either pathway. Could this feat ever be accomplished? Marshall et al. noted high expression of putative O_2-reducing cytochromes in an electrosynthetic acetate-producing microbial community despite the absence of O_2. This result could suggest that the Wood-Ljungdahl

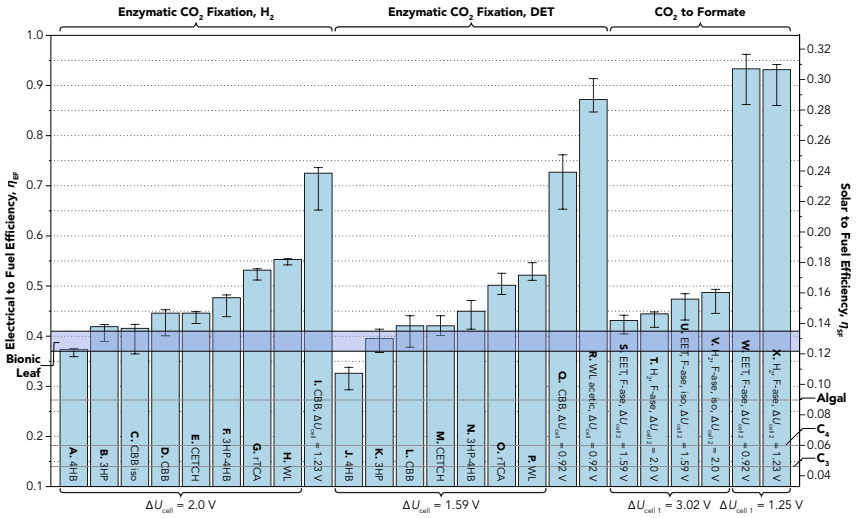

Figure 4. Projected Lab-Scale Electrical and Solar to Biofuel Efficiency of Electromicrobial Production Schemes

The right axis is calculated by assuming a solar to electrical conversion efficiency of 32.9%, the maximum efficiency of a single-junction Si solar PV. [66] Bars S to V assume a faradic efficiency of CO_2 to formate reduction of 80%, while bars W and Z assume 100% faradic efficiency. Whole-cell voltages were calculated from the minimum redox potentials of H_2 and the Mtr EET complex [113] midpoint redox potentials and from bias voltages reported by [23,24,72] Metabolic pathway data can be found in Table S2. All efficiencies are for butanol production, except where noted as isopropanol (iso) or acetic acid. This plot can be recreated with the fig-co2fixation.py program and fig-co2fixation.csv input file in the REWIREDCARBON package. 4HB, 4-hydroxybutyrate cycle; 3HP, 3-hydroxypropionate bicycle; CBB, Calvin-Benson-Bassham cycle; CETCH, (CoA)/ethylmalonyl-CoA/hydroxybutyryl-CoA; 3HP-4HB, 3-hydroxypropionate 4-hydroxybutyrate bicycle; rTCA, reductive tricarboxylic acid cycle; WL, Wood-Ljungdahl pathway. Error bars are due to uncertainity in trans-inner membrane voltage. The error bars span efficiency estimates for $\Delta U_{membrane}$= 80 mV (BioNumbers ID (BNID) 104082[84]) to 270 mV (BNID 107135), with a central value of 140 mV (BNIDs 109774, 103386, and 109775).

pathway could be used in concert with oxygen reduction. Filamentous N_2-fixing cyanobacteria are able to operate the highly O_2-sensitive nitrogenase enzyme inside O_2-impermeable differentiated cells called heterocysts while simultaneously operating oxygenic photosynthesis to generate reducing equivalents in adjacent cells.[90] A similar approach, or recent advances in compartmentalization in synthetic biology,[91–93] may enable the implementation of these highly efficient CO_2-fixation pathways in synthetic organisms that simultaneously use O_2 as a metabolic terminal electron acceptor. However, achieving this goal is likely to represent a major challenge in synthetic biology.

H_2-Mediated Electromicrobial Production Reaches Its Maximum Efficiency in Large-Scale Systems

In principle, the efficiency of an EMP system could be independent of the specific activity of the carbon fixation pathway used (how many CO_2 molecules are fixed each second by each gram of enzyme). Fixing more CO_2 and storing more energy might simply require more cells operating in parallel. However, despite its advantages as a mediator[18] the low solubility of H_2 in water means that distributing electrical power through a H_2 mediator is likely to pose energetic, geometric, and safety challenges.[60–62] To assess these challenges, we built models of H_2 transport by diffusion and agitation.

The difficulty of H_2 transport is determined by the number and volume of cells needed to store the H_2 current, I_{H_2}, produced by the cell current (ξ_{eH_2} is the faradic efficiency of H_2 production, typically close to 1):

$$I_{H_2} = \xi_{eH_2} I_{cell}. \quad \text{(Equation 5)}$$

Note that this model does not consider the financial cost of H_2 production but does consider the energetic cost through the faradic efficiency, ξ_{eH_2}, and the whole-cell voltage, ΔU_{cell}, as well as the transport costs.

As hydrogenase enzymes are much faster than any carboxylating enzyme, the CO_2 fixation rate is the limiting factor in electron demand per cell. The rate of electron uptake by each cell depends on the number of electrons, ν_{ef}, and carbon atoms fixed, $\nu_{Cf,fix}$ (not just the number incorporated, ν_{Cf}), to synthesize each fuel molecule; and the rate and number of carbon-fixing enzymes, r_{fix} and ν_{fix} (Supplemental Experimental Procedure 3):

$$\dot{\nu}_e = \nu_{ef} r_{fix} \nu_{fix} \Big/ \nu_{Cf,fix}. \quad \text{(Equation 6)}$$

Thus, the total number and volume of cells needed to store the H_2 current (n_{cells} is the cell density):

$$N_{cells} = I_{H_2} \Big/ e\dot{\nu}_e, \quad \text{(Equation 7)}$$

$$V_{cells} = N_{cells} / n_{cells}. \quad \text{(Equation 8)}$$

H_2 could be transported by diffusion from the headspace of a reactor (where it is at a partial pressure P_{H_2}) without any additional energy input into the system (Figure 5A). In order to achieve the high concentration gradient needed to drive rapid diffusion of H_2 (D_{H_2} and k_{H_2} are the diffusion and solubility coefficients for H_2, respectively), the cell culture has to be spread into a film with a height no greater than and an area no less than (Supplemental Experimental Procedure 4):

$$h_{film} \leq \sqrt{\left(\left(2 P_{H_2} D_{H_2} N_A\right) \Big/ \left(k_{H_2} n_{cells} \dot{\nu}_e\right) \right)}, \quad \text{(Equation 9)}$$

$$A_{film} \geq \frac{\xi_{eH_2} k_{H_2}^{1/2} P_{e,avail}}{e \Delta U_{cell} \left(2 \dot{\nu}_e n_{cells} P_{H_2} D_{H_2} N_A\right)^{1/2}}. \quad \text{(Equation 10)}$$

The area of an EMP system supplied by H_2 diffusion scales linearly with input power while the film thickness remains the same. *R. eutropha* is typically grown under an atmosphere containing H_2, O_2, and CO_2 at a ratio of 8:1:1.[94] At the laboratory scale, the H_2 partial pressure is usually restricted to 5% of a total pressure of 1 atmosphere in order to reduce the risks of H_2 explosion.[94] If supplied by a solar photovoltaic (PV), the area of the film relative to the solar PV area, A_{PV}, will remain constant. A plot of film thickness and area versus cell culture density is shown for two systems supplied by a 1 m^2 solar PV in Figure 5B: the first with a headspace H_2 partial pressure of 5,066 pascals (Pa) (5% of 1 atmosphere; O_2 and CO_2will both be at a partial pressure of 633.25 Pa, and the system will be balanced with N_2), and the second with a H_2 partial pressure of 81 × 10^6 Pa (80% of 1,000 atmospheres; O_2 and CO_2 will both be at a partial pressure of 10.1 × 10^6 Pa).

For the ambient pressure system, the film area (and potential footprint of the system) is greater than the area of the PV supplying it for even the highest cell densities seen in bio-industrial applications. At the highest reported autotrophic density for *R.*

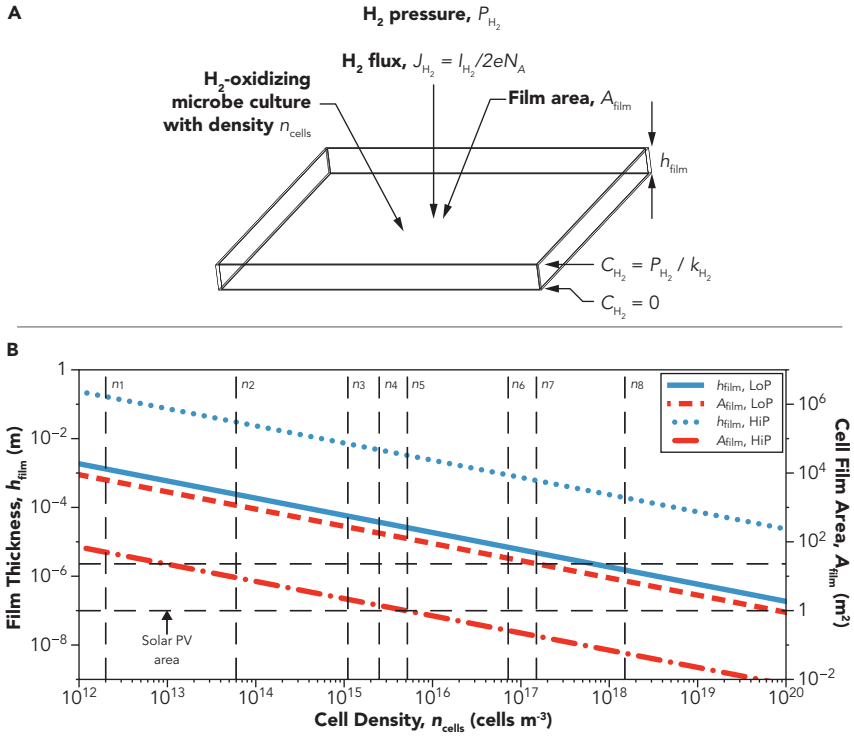

Figure 5. H_2 Transport by Diffusion to Enable Scale-Up of H_2-Mediated Electromicrobial Production Systems Using the Calvin Cycle (CBB) to Convert CO_2 to Butanol, Model 1 in Table 1

(A) Geometry for H_2 mixing by diffusion.

(B) Maximum height of cell culture that can be supplied with H_2 by diffusion and corresponding area of culture needed to convert 330 W of electrical power (produced by a perfectly efficient 1 m^2 single-junction Si solar PV illuminated by 1,000 W of solar power) at H_2 partial pressures of 5,066 Pa (5% of atmospheric pressure; LoP) and 81 MPa (80% of 1,000× atmospheric pressure; HiP). Eight important cell density regimes are noted in Supplemental Experimental Procedure 5 and Table S3, and the average of each regime is shown with a dashed line here in (B): n_1: maximum cell density of the psychro- and barophilic strain F1-A at 45.6 MPa (450× *atmospheric pressure*) (grown at 3°C)[141]; n_2: cultures of *E. coli* grown aerobically at 37°C in the laboratory on LB media in exponential phase (BNID 100985); n_3: batch-cultures strain of thermophile, *C. saccharolyticus*, grown anaerobically at 70°C on sucrose[142]; n_4: cultures of hyperthermophilic strain, *P. abyssi*, at 90°C[144]; n_5: cyanobacteria grown autotrophically to maximum density[145]; n_6: cultures of *E. coli* grown aerobically at 37°C on LB media at saturating density (BNID 104940); n_7: H_2-oxidizing microbe *R. eutropha* grown autotrophically on CO_2, H_2, and O_2 to maximum density at 30°C[95]; and n_8: saturating cultures of yeast grown aerobically in an industrial bioreactor (Abbas, C. personal communication) (B) can be recreated with the fig-h2diffusion.py programs and corresponding input file in the REWIREDCARBON package. To ease interpretation of (B) we have re-drawn this panel as two separate panels, each with a single curve representing the area and thickness of the cell culture film at each pressure in Figure S7.

eutropha (density region 7; *n*7),[95] the film area is between 20 and 28 m^2. It is unclear if the large film area requirements for H_2 transport by diffusion at ambient pressures are surmountable. Possible approaches to the construction of a bioreactor with a high internal area but relatively small external footprint include stacking planar cell layers on top of one another, or using hollow fibers in which cells are immobilized on the walls of the fiber and reactant gases are flowed along its inner and outer surfaces such as those developed by Worden and Liu.[96] However, significant detailed modeling will likely be required before recommending and pursuing any particular approach.

Furthermore, by increasing the H_2 partial pressure to 81 × 10^6 Pa, the cell film area can be reduced to 1 m^2 by a density of ≈5 × 10^{15} cells m^{-3}, inside the range of typical cyanobacterial cell densities (density region 5; *n*5).

H_2-diffusion systems could enable very high efficiency but may come at the cost of high initial expenditure, complexity, maintenance, potential for H_2 escape, and difficulty in removing product.

The diffusion analysis can also be applied to system in which H_2 is delivered to the cell culture by a micro-sparger at the bottom of a bubble column. In this case, the inter-bubble spacing can be approximated by the film thickness (9), the total bubble surface area can be approximated by the film area (Equation 10); and the total bubble volume passing through the culture per second can be approximated by:

$$V_{H_2} = \left(I_{H_2} k_B T\right) / \left(2 e P_{H_2}\right) \quad \text{(Equation 11)}$$

Intuitively, agitation allows H_2-transport without the need for extreme system geometries, high pressures, or both, at the expense of power input. The input power to the electrochemical cell is the total available electrical power, $P_{e,total}$, minus any power needed to agitate the system:

$$P_{e,avail} = P_{e,total} - P_{e,stir}. \quad \text{(Equation 12)}$$

We considered a cylindrical stirred tank of cells that continuously distributes H_2 supplied by a sub-surface pipe (Figure 6A). We numerically solved a set of coupled equations linking H_2 production, consumption, gas transfer rate, cell culture volume, and the power required for gas mixing through an iterative algorithm in the REWIRED-CARBON package using a formalism compiled by Van't Riet[97] until a self-consistent set of solutions were found (Supplemental Experimental Procedure 6). The solution to these equations for a system supplied with 330 W of electrical power from a 1 m^2 solar PV are plotted in Figures 6B–6D.

At low cell densities and high system footprints (and hence volumes), the power required to transport H_2 is low, while at low volumes the effort to stir is much greater (Figure 6B). This corresponds with intuition that suggests that turbulent mixing, which is favored in larger systems due to a higher Reynolds number, is more effective than laminar mixing, which predominates in smaller-scale systems. This creates a conundrum, $P_{e,stir}$ can be minimized, but at the expense of a tank footprint much larger A_{PV}. Or, the tank footprint can be reduced to less than A_{PV} but at the expense of diverting more and more solar power to mixing H_2 (Figure 6B). This means that the efficiency of the EMP system (Figure 6C) drops precipitously from its maximum potential value to almost zero as the footprint of the system is reduced to allow it to fit under the solar PV supplying it.

The footprint-efficiency dilemma can be resolved by operating at higher input power. We calculated the system footprint to PV area ratio (A_{tank}/A_{PV}) at which the system achieves 50%, 75%, and 95% of its maximum potential efficiency in Figure 6D. For small-scale systems (500 to 10^4 W of solar power) footprints of 60× to 7× the area of the solar PV supplying them are required to achieve 75% of maximum efficiency. However, for large scales systems exceeding 1.1 × 10^5 W of electrical power, the system footprint begins to shrink below that of the solar PV supplying it. Systems supplied by more than 1.1 × 10^6 W of electrical power can achieve 95% of maximum efficiency and still have a footprint smaller than the solar PV supplying them.

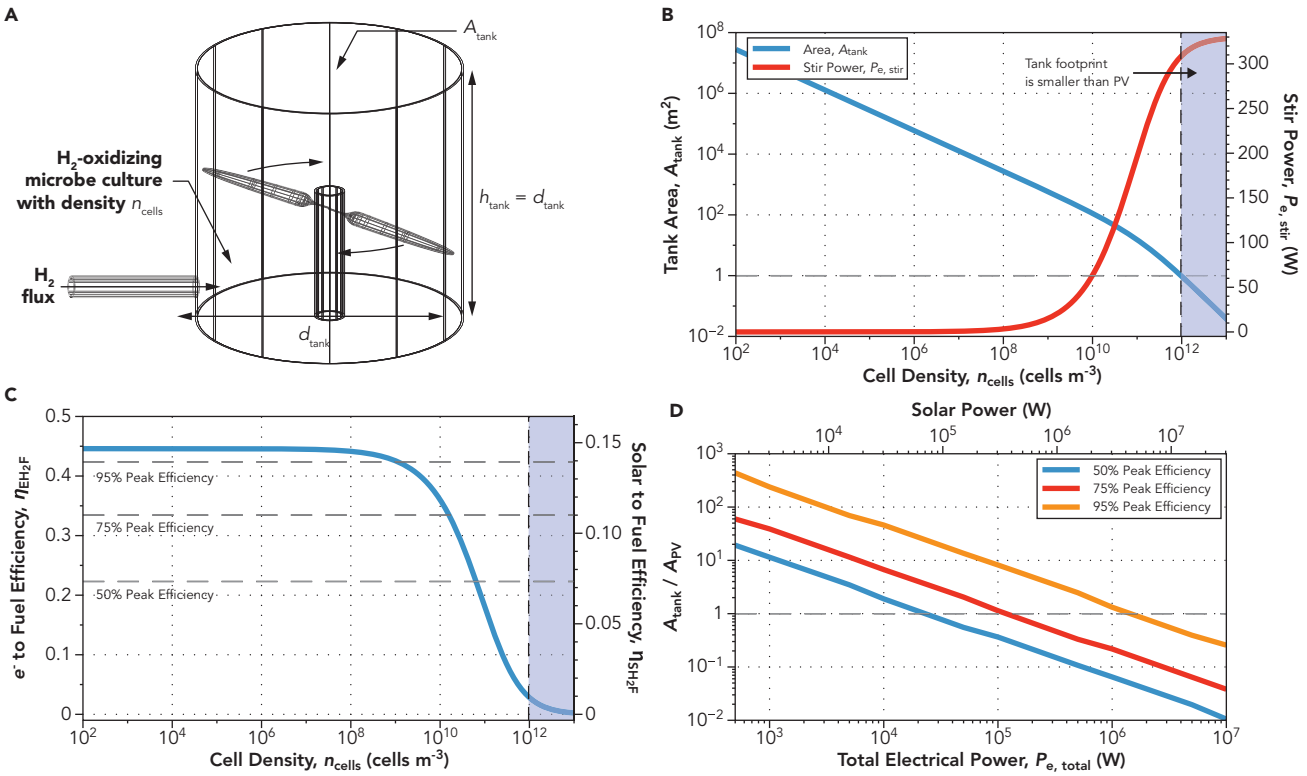

Figure 6. Scale-Up of H_2-Mediated Electromicrobial Production Systems Using the Calvin Cycle (CBB) to Convert CO_2 to 1-Butanol, Model 1 in Table 1

(A) Geometry for mixing H_2 by agitation. Note that this reactor may require additional media inlets and outlets for culture maintenance.

(B) As cell density is increased to reduce system footprint, the power required to mix H_2 by agitation increases, eventually consuming all of the 330 W available to the system, (C) reducing the electricity to fuel efficiency to zero.

(D) But, the system footprint to PV area ratio at which the system achieves 50%, 75%, and 95% of its peak efficiency falls with increasing input power to the system (and solar PV area). (B) to (D) in this plot can be recreated with the fig-h2agitation-(B) to (D).py programs and the corresponding input files in the REWIREDCARBON package. Note that the cell densities shown here are much lower than those highlighted in Figure 5.

DET Matches the Efficiency of H_2 and Can Achieve High Efficiencies at Small Scales

Electron Requirements for Fuel Synthesis in a Reverse Electron Transport System

DET could allow scale-up of EMP through the use of a conductive biofilm to supply electrons to the cell (Figure 1C). Electroactive microbes can transfer charge to, from, and between external substrates like metals and even electrodes at distances up to a centimeter from the cell surface and use specialized metalloprotein complexes that connect the cell surface to the electron transport chain in the inner membrane (Figure 2B).[98–101]

The energy landscape of DET has raised concerns about its use in EMP. The redox potentials of the membrane spanning cytochrome complex (Mtr in *S. oneidensis* at ≈−0.1 V versus the standard hydrogen electrode [SHE][102]) and the inner membrane electron carriers menaquinone (−0.0885 V[102]) and ubiquinone (0.1 V[102]) are too high to directly reduce NAD^+ to NADH (−0.32 V[103])

Nature suggests that the redox potential mismatch between the inner membrane and NAD^+ is not insurmountable. Today, electroactive micro-aerophilic neutrophilic iron-oxidizing microbes like *Sideroxydans lithotrophicus* are able to draw electrons from the oxidation of iron minerals at redox potentials from +0.7 to ≈0.1 V to power

CO_2-fixation and autotrophic metabolism.[104,105] Furthermore, the electroactive iron-oxidizing microbe *Mariprofundus ferrooxydans* PV-1 can even be cultured on an electrode poised at −0.076 V.[106] In the distant past it is thought that iron oxidation powered the global carbon cycle.[107] It is speculated that an "uphill pathway" is able to lower the redox potential of electrons in the quinone pool to that of NAD^+.[102]

Recently, Rowe et al.[108] provided compelling evidence that a reverse electron transport chain providing an uphill pathway operates in *S. oneidensis*. While the full complement of genes encoding this pathway remains unknown (although some parts have been found),[108–111] this pathway is proposed to operate by directing part of a cathodic current downhill in energy to a terminal electron acceptor (in this case, assumed to be O_2) and pumping protons across the inner membrane. The energy stored in the proton gradient is used to power NAD^+ reduction (and potentially ferredoxin reduction, too) (essentially the electron acceptor for reverse electron transport) and ATP production. A model for electron uptake by DET is shown in Figure 2B. It should be noted that as of today there is no known easily genetically engineered microbe capable of both electron uptake by DET (often referred to as reverse electron transport) and CO_2 fixation. At the time of writing, it is unknown why *S. oneidensis* is capable of reverse electron transport. This process may allow *S. oneidensis* to acquire energy for cellular maintenance in the absence of a carbon source, but we stress that this is pure speculation. The following discussion considers a possible highly engineered microorganism capable of both reverse electron transport and CO_2 fixation. However, at the time of writing, we are aware of very few efforts to model the reverse electron transport process,[112] and none that incorporate it into a start (electricity and CO_2) to finish (biofuel) model of EMP.[17]

Due to the need to sacrifice some current to generate a proton gradient for NAD^+ (and possibly Fd) reduction, the number of electrons needed to produce the NADH, Fd, and ATP for synthesis of a single fuel molecule through DET is higher than in H_2 oxidation (a full derivation is included in Supplemental Experimental Procedure 7):

$$\begin{aligned} \nu_{ef,EET} = & \\ & 2\nu_{f,NADH} + 2\nu_{f,Fd} \\ & + \nu_{f,ATP}\frac{ceil\left(\Delta G_{ATP/ADP}/e\Delta U_{membrane}\right)}{floor\left(\left(U_Q - U_{Acceptor}\right)/\Delta U_{membrane}\right)} \\ & + 2\nu_{f,NADH}\frac{ceil\left(U_{NADH} - U_Q/\Delta U_{membrane}\right)}{floor\left(\left(U_Q - U_{Acceptor}\right)/\Delta U_{membrane}\right)} \\ & + 2\nu_{f,Fd}\frac{ceil\left(U_{Fd} - U_Q/\Delta U_{membrane}\right)}{floor\left(\left(U_Q - U_{Acceptor}\right)/\Delta U_{membrane}\right)}. \end{aligned} \quad \text{(Equation 13)}$$

However, counterintuitively, DET-mediated EMP is not dramatically less efficient than H_2-mediated EMP (Figure 4). While the number of electrons needed to produce a molecule of fuel is higher in a DET-mediated system than in an otherwise comparable H_2-mediated system using the same CO_2-fixation pathway, the whole-cell voltage in a DET-mediated system is lower than in a H_2-mediated system ($\Delta U_{cell} \geq 1.23$ V for H_2 but only ≥ 0.92 V for DET) as the redox potential of Mtr is much lower than H_2.[113] Furthermore, the bias voltages at lab-scale remain approximately the same,[7] meaning more total current is available to a DET-mediated system. However, DET-mediated EMP is approximately twice as sensitive to changes in transmembrane voltage than a H_2-mediated system (Figure S1). How far the efficiency of direct electron uptake from this maximum depends upon how many protons can be

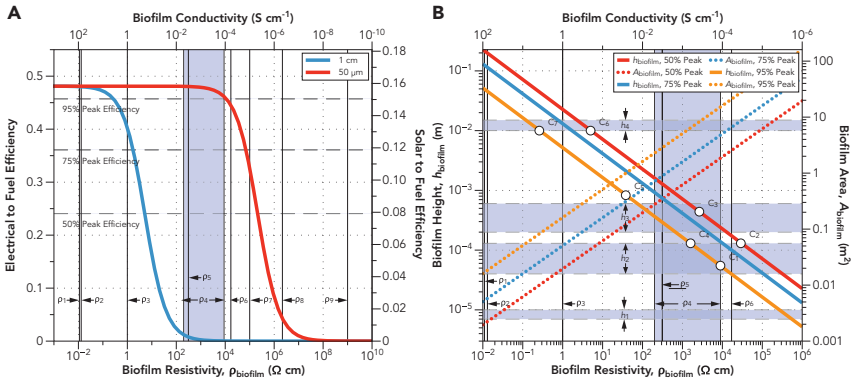

Figure 7. Biofilm Resistivity Determines Efficiency Losses in the Scale-Up of DET-Mediated Electromicrobial Production, Model 2 in Table 1

(A) The system shown here has an anode bias voltage of 0.47 V, fixes CO_2 with the Calvin cycle and produces butanol (A). The electrical to fuel efficiency of an EMP system drops after a threshold resistivity is reached. The thicker the biofilm, the earlier this drop occurs.

(B) Maximum biofilm thickness and minimum area needed to achieve 50%, 75%, and 95% of peak efficiency. This plot can be recreated with the fig-EETscaleup- A.py and B.py programs and corresponding input files in the REWIREDCARBON package. Representative conductive matrix resistivities and heights: ρ_1, high conductivity polypyrrole[126]; ρ_2, individual cable bacteria filaments[124]; ρ_3, individual *S. oneidensis* nanowires[123]; ρ_4, bulk *G. sulfurreducens* and *S. oneidensis* biofilm resistivities[116,121,122]; ρ_5, polypyrrole conductive matrix for *S. oneidensis*[127]; ρ_6, *Marinobacter-Chromatiaceae-Labrenzia* (MCL) electroautotrophic cathode biofilm[16]; ρ_7, bulk *E. coli* biofilm[150]; ρ_8, HBr doped polyaniline[153]; ρ_9, low conductivity polypyrrole[126]; h_1, MCL electroautotrophic biofilm; h_2, *G. sulfurreducens* biofilms; h_3, polypyrrole conductive matrix for *S. oneidensis*; h_4, cable bacteria biofilms and individual filaments (Supplemental Experimental Procedure 9 and Tables S4 and S5). To help interpretation of (B) we have re-drawn this panel as three separate panels, each with a single curve representing the area and thickness of the biofilm at each efficiency in Figure S8. We have highlighted seven speculative biofilm configurations (C_1 to C_7) in white circles that are summarized in Table 2.

pumped from the cytosol into the periplasm relative to the maximum possible. The effect of limiting the number of proton-pumping events is shown in Figure S9.

Energy Losses in a Conductive ECM

The scale-up of DET-mediated EMP is potentially much easier than H_2 -EMP. We built a model of scale-up for a DET-mediated system assuming that the dominant source of overpotential is the resistivity of the biofilm. Simply put, the smaller the area of the conductive ECM, the easier (and cheaper) it will potentially be to construct an EMP reactor. The smaller the area of the biofilm, the thicker it needs to be (the same number of cells can either be arranged in a short wide-area biofilm, or thick low-area biofilm). However, the thicker the biofilm is, the higher its resistance will be, the greater the energy losses suffered in transporting electrons across the conductive ECM will be, and the lower the overall energy conversion efficiency.

This section aims to specify the biofilm resistivity needed to achieve a given acceptable energy conversion efficiency for a system with a specified internal area (and hence biofilm thickness). We illustrate this with seven ECM configurations highlighted in Figure 7B and summarized in Table 2. We do not specify how these resistivities will be achieved (i.e., what the conduction mechanism needs to be metallic, redox gradient, or something else), but we do reference naturally occurring and synthetic systems in which these resistivities and thicknesses have been observed, either together or separately. One could think about this section as an answer to the question: if I know what internal area is acceptable for a viable bioreactor, what

Table 2. Representative Conductive ECM Configurations

Configuration	% of Peak Efficiency	Electrical to Biofuel Efficiency (%)	Resistivity (Ω cm)	Thickness (μm)	Area (m^2)
C1	45.7	95	8,952	55	15
C2	24.1	50	29,000	130	3.4
C3	24.1	50	2,650	440	1
C4	45.7	95	1,600	130	6.4
C5	45.7	95	38	830	1
C6	24.1	50	5	104	0.044
C7	45.7	95	0.26	104	0.079

Summary of conductive ECM area, height, resistivity, and corresponding electrical-to-biofuel conversion efficiency configurations shown in Figure 7B.

combination of biofilm thickness and resistivity can I get away with? Alternatively: if I know I can only make a biofilm with a given thickness and resistivity, what internal area do I have to build into my reactor to achieve a chosen efficiency?

This model of scale-up of a DET-mediated EMP system relies upon a simplified version of the framework for biofilm conduction laid out by Korth and Harnisch.[17] First, while stratification of metabolic activity has been observed in naturally evolved anode biofilms,[114] we introduce the constraint that each cell in the biofilm receives sufficient current to operate at its maximum possible metabolic rate, set by its CO_2-fixation rate ($6.2 \times 10^7 e^- cell^{-1} s^{-1}$, or 9.9 pA $cell^{-1}$, for butanol production with the Calvin cycle, see Supplemental Experimental Procedure 3). Second, we make the assumption that electron transport across the conductive biofilm is a one step process.[17] Third, while the redox gradient model appears to most accurately describe electron conduction in naturally occurring electroactive biofilms,[115–119] Korth and Harnisch[17] and Ing et al.[120] note that low conductivity biofilms can be treated as Ohmic conductors for the purposes of calculating the voltage needed to drive a given current across the biofilm. Thus, the bias voltage needed to transport the minimum current (I_{cell}) needed to produce maximum metabolic activity even in the cell furthest from the electrode is:

$$\Delta U_{biofilm} = \rho_{biofilm} h_{biofilm} I_{cell} / A_{biofilm}. \quad \text{(Equation 14)}$$

We developed a set of five coupled equations to solve for the cell current I_{cell}, the bias voltage needed to drive current across the biofilm $\Delta U_{biofilm}$, the area of the biofilm $A_{biofilm}$, the total number of cells in the biofilm N_{cells}, and the volume of the biofilm $V_{biofilm}$ in Supplemental Experimental Procedure 8. These equations were solved numerically, and the results are shown in Figure 7. Unlike agitation-based systems, the energy cost of electron transport by DET scales linearly with system size: for a given biofilm resistivity, the ratio of the areas of the biofilm and the solar panel supplying it with electricity remains constant. Moreover, there is no obvious penalty for operating small-scale systems as there is with agitation.

At low resistivities (high conductivities) the biofilm overpotential is small, allowing a conductive matrix system to achieve close to its maximum possible efficiency, set only by the thermodynamic minimum voltages and any non-biofilm bias in the system (Figure 7A). However, above a critical resistivity, the efficiency drops precipitously. For a 50 μm thick film, the efficiency starts to drop below 95% of maximum at a resistivity of $\approx 10^5$ Ω cm, considerably higher than the commonly reported resistivities of *Geobacter sulfurreducens* and *S. oneidensis* biofilms (ρ_4 in Figure 7A,

Supplemental Experimental Procedure 9).[116,121,122] Note that the peak efficiency shown in Figure 7A exceeds that shown in Figure 4 bar L as we assume only anode bias initially (the cathode bias grows as the biofilm thickness increases).

As the resistivity of the conductive matrix increases, its thickness must decrease and its area must increase in order to maintain a given efficiency. In contrast to a 50 μm film, a 1 cm thick film suffers a drop in efficiency to 50% of maximum at a resistivity of only ≈10 Ω cm, well below the resistivity range of *G. sulfurreducens* and *S. oneidensis* biofilms[116,121,122] but above the reported resistivities of individual *S. oneidensis* nanowires (ρ_3 in Figure 7A)[123] and individual filaments produced by the cable bacterium *Thiofilum facile* (ρ_2 in Figure 7A).[124]

Figure 7B shows the maximum conductive matrix thickness and minimum area able to achieve a given fraction of peak efficiency as a function of resistivity. We have highlighted seven configurations of ECM area, thickness, resistivity, and their corresponding electrical-to-biofuel conversion efficiency in Figure 7B and summarized them in Table 2. We believe that the first three configurations (C_1 to C_3), with high areas, low thicknesses, and higher resistivities are readily achievable, given natural precedent. On the other hand, the fourth configuration (C_4) is at the edge of what is presently achievable, while the last three (C_5 to C_7) are more speculative and will require significant advances in biofilm engineering. However, we do believe that they may fall within the realm of possibility.

Biofilm Configuration C_1: If 95% of peak efficiency (45.7% electrical-to-biofuel conversion efficiency, assuming no additional cathode bias) were desired, but only a thin biofilm of 55 μm with a high resistivity of 8,952 Ω cm could be produced, then a biofilm area of 15 m^2 would be needed.

Biofilm Configuration C_2: If a film thickness of 130 μm can be achieved (well within the range of commonly observed *G. sulfurreducens* and *S. oneidensis* biofilm thicknesses), then the biofilm area could be decreased to 3.4 m^2, with a high biofilm resistivity of 29,000 Ω cm (above that of many conductive biofilms, perhaps allowing some conductivity to be sacrificed to enable increased CO_2 inflow or biofuel outflow) if 50% of peak efficiency (24.1% electrical to biofuel) is acceptable.

Biofilm Configuration C_3: If 50% of peak efficiency is still acceptable, then the biofilm area can be constrained to 1 m^2 (equal to that of the solar PV supplying it) if the biofilm resistivity is reduced to 2,650 Ω cm, well within the range of *G. sulfurreducens* and *S. oneidensis* biofilm resistivities. However, the corresponding film thickness is 440 μm, about 3× the height of most commonly observed *G. sulfurreducens* and *S. oneidensis* biofilms (although Renslow et al. did observe *S. oneidensis* films as thick as 450 μm). However, artificial polypyrrole conductive ECMs have been produced that are as thick as 600 μm and have resistivities as low as 312 Ω cm (ρ_5 in Figure 7).

Biofilm Configuration C_4: On the other hand, if a thickness of 130 μm and resistivity of 1,600 Ω cm are simultaneously achievable, 95% of peak efficiency can be achieved if a 6.4 m^2 biofilm area is acceptable. We believe this configuration (resistivity and thickness) may be just possible with current knowledge and technology.

If low conversion efficiency (≈50% of peak) or high internal area (≥1 and <≈15× the area of the solar PV supplying the reactor) (or both) is acceptable, then naturally

occurring biofilms like those produced by *S. oneidensis* and *G. sulfurreducens* already supply the necessary resistivities and thicknesses.

Biofilm Configuration C_5: If a 1 m^2 biofilm with a resistivity 38 Ω cm and a thickness of 830 μm could be produced, 95% of peak efficiency could be achieved.

Biofilm Configuration C_6: If a biofilm could be produced with a 1 cm thickness and an area of only 0.044 m^2 then 50% of maximum efficiency could be achieved.

Biofilm Configuration C_7: If a biofilm of 1 cm thickness, with a resistivity of 0.26 Ω cm, and an area of 0.079 m^2, 95% of peak efficiency could be achieved.

If low internal area ($\leq 1\times$ the area of the solar PV supplying the system) or high efficiency ($\approx$95% of peak) (or both) are desired, high biofilm thicknesses ($\approx$1 cm) and very low resistivities ($< \approx$50 Ω cm) will be required in combination. Are these high thicknesses and low resistivities possible, even in isolation? Individual *S. oneidensis* nanowires have a resistivities of 1 Ω cm (at least when on an electron microscopy grid).[123] Meanwhile, individual *T. facile* (a species of cable bacteria) filaments can have resistivities as low as 1.3×10^{-2} Ω cm, over lengths of up to 10.1 mm [124] (h_4 and ρ_2 in Figure 7).

Is it possible to produce an entire biofilm that is $\approx$1 cm thick and with a resistivity similar to (almost certainly not necessarily equal, but not orders of magnitude less either) those of individual *T. facile* or *S. oneidensis* filaments? Cable bacteria are capable of producing $\approx$1cm thick biofilms,[125] so high thickness has natural precedent. However, we are unaware of any naturally occurring biofilm with an overall resistivity of $\leq$200 Ω cm (a *G. sulfurreducens* film with a thickness of approx. 100 μm[116]).

Could artificial conductive organic polymers point the way toward a high thickness low resistivity biofilm? Polypyrrole, depending upon preparation technique, can have a resistivity as low as 1.1×10^{-2} Ω cm.[126] Furthermore, Yu et al. constructed an artificial conductive matrix for *S. oneidensis* from polypyrrole with a resistivity of 312 Ω cm with a thickness of 200 to 600 μm.[127] Taken together, these data points suggest that a high thickness, low resistivity film is possible. Would it be possible to synthesize such a film biologically, to enable self-assembly and self-repair? Recent advances in computational protein design might enable design of enzymes that can synthesize and secrete a conductive polymer with similar properties to polypyrrole. Achieving this is likely to be a grand challenge in biofilm engineering but may be within the realm of possibility.

On a final practical note, it is likely that any biofilm used in scaled-up DET-EMP will need to be cultivated prior to the culture switching into a CO_2-fixing and product-synthesizing mode. Furthermore, these high biofilm thicknesses could need elaborate cultivation and maintenance strategies. For example, continuous chemostat cultivation may be needed to at least provide trace element needs, if not also fixed carbon and nitrogen for an initial heterotrophic growth phase. Alternatively, batch growth or even solid media strategies may be required.

Electrochemical CO_2 Fixation Could Allow Very High Electricity to Fuel Conversion Efficiencies

H_2-oxidation and DET could be an important complement to electrochemical CO_2-fixation technologies. Current electrochemical CO_2-fixation systems typically

produce compounds with no more than two carbons that are often not completely reduced.[73] By contrast, most drop-in fuels require at least 2 to 3 carbons, with 8 electrons each.

Li et al. demonstrated the reduction of formate to isobutanol and 3-methyl-1-butanol (3MB) by the H_2-oxidizing microbe *R. eutropha*.[22] While this work relied upon oxidation of formate to CO_2 and subsequent re-fixation by RuBisCO, recent advances in artificial computational metabolic pathway could enable enzymatic transformation without reliance upon this bottleneck.[128,129]

The efficiency of electrochemical CO_2-fixation EMP schemes is set by the number of electrons $\nu_{e,add}$ needed to produce the NAD(P)H, Fd, and ATP needed to transform the primary fixation product to a biofuel; the charge needed to synthesize the primary electrochemical CO_2-fixation product, $e\nu_{ep}$; the number of carbons in each primary fixation product, ν_{Cp}; the faradic efficiency of the first electrochemical reaction, ξ_{I1}, (while we are calculating an upper limit on efficiency we have rarely seen $\xi_{I1}>0.8$[73]); the efficiency of carbon transfer to the second cell ξ_C; and the faradic efficiency in the second cell ξ_{I2}(Supplemental Experimental Procedure 10):

$$\eta = \frac{P_{e,avail} E_{fuel} \xi_{I2}}{e\nu_{e,add}\left(\Delta U_{cell1}\left(\frac{\nu_P \nu_{ep} \nu_{Cp} \xi_{I2}}{\xi_{I1} \xi_C \nu_{e,add}}\right) + \Delta U_{cell2}\right) P_{input,total}}. \quad \text{(Equation 15)}$$

Even with only 80% faradic efficiency for the conversion of CO_2 to formate, the electrical energy to butanol conversion efficiency of the formolase artificial metabolic pathway[128] powered by either H_2-oxidation or EET exceeds all fully enzymatic CO_2-fixation pathways with the exception of the rTCA cycle and Wood-Ljungdahl pathway Figure 4 and suffers no complications of O_2-sensitivity.

Conclusions

What combination of electron uptake, electron transport, and carbon fixation is the best for EMP? The model of EMP lets us sketch out a roadmap for how to proceed with the technology. We outline 10 possible development and deployment scenarios that could be pursued in the near and further future in Table 3 along with their advantages, disadvantages, and suggested niche.

This work shows that H_2 EMP using the Calvin cycle[23,24] is already highly optimized. This means that engineering the host microbe (e.g., *R. eutropha*) by adjusting expression levels of enzymes already encoded in the genome or changing the transmembrane voltage (Table 3, scenario 8) are unlikely to produce gains of more than a few percentage points in electricity to biofuel conversion efficiency.

One genetic engineering route to increased electrical-to-biofuel conversion efficiency (from ≈40 % to as high as 55% at lab scales) is the incorporation of any one of the CETCH, 3HP-4HB, rTCA, or WL CO_2-fixation pathways (Table 3, scenarios 2 and 7). Although this approach may not be for the faint hearted, recent impressive progress in engineering the Calvin cycle into *E. coli* makes this a tantalizing possibility.[29,130] While incorporation of the rTCA or WL pathways would yield the greatest increase in efficiency, the need to use O_2 as a terminal electron acceptor to achieve maximum efficiency means that the O_2-sensitivity of these pathways will need to be mitigated. However, incorporation of the CETCH or 3HP-4HB pathways would allow for an ≈10% increase in electrical-to-biofuel conversion efficiency over what has been demonstrated in the lab.[24]

Table 3. Future Research and Development and Deployment Scenarios for Electromicrobial Production.

#	Scenario	Advantages	Drawbacks	Display Item
1	Metabolically engineer *R. eutropha* by adjusting enzyme expression.	Straightforward genetic engineering.	Unlikely to produce significant gains in electricity to biofuel conversion efficiency.	Figures 4C and 4D
2	Engineer H_2-oxidizing chassis with more efficient CO_2 fixation.	Significant increase in electrical to bio- fuel conversion efficiency.	Significant increase in genetic engineering complexity. O_2-sensitivity (rTCA and WL).	Figures 4E–4H
3	Engineer H_2-oxidizing chassis with formate assimilation pathway.	Significant increase in electrical-to-biofuel conversion efficiency. Less complex genetic engineering. No known O2-sensitivity issues.	Increased system complexity due to electrochemical CO_2 reduction.	Figures 4T and 4V
4	Deploy H_2-EMP in large volume stirred tank reactor at ambient pressure.	Small footprint. Low system complexity.	Potential for H_2 escape and energy loss. Only efficient at large scales ($\geq$ 1 MW).	Figure 6
5	Deploy H_2-EMP in a diffusional hollow fiber reactor at ambient pressure.	Efficient at all power scales.	High reactor complexity due to large in- ternal surface area. Potential for H_2 escape and energy loss.	Figure 5B
6	Deploy H_2-EMP in a diffusional hollow fiber reactor at high pressure.	Efficient at all power scales. Significantly reduced internal area compared with ambient pressure case.	Increased complexity due to need to maintain high internal gas pressure. Explosive atmosphere. Potential for H_2 escape and energy loss.	Figure 5B
7	Engineer DET chassis with CO_2-fixation pathway.	No volatile intermediate (H_2).	Small efficiency loss compared with H_2-oxidizing chassis organism. Highly complex genetic engineering.	Figure 4, bars L–O and 4P
8	Engineer DET chassis with a formate assimilation pathway.	Potential significant increase in electrical-to-biofuel conversion efficiency over a chassis using the CBB cycle. Less complex genetic engineering. No known O_2-sensitivity issues.	Increased system complexity due to electrochemical CO_2 reduction.	Figure 4, bars S and U
9	Deploy DET-EMP with a conductive ECM.	No volatile intermediate (H_2). Potential for low internal area reactor. Room for reduction in ECM conductivity to allow CO_2 access and product extraction.	Small efficiency loss relative to H_2-transport. Potential difficulty in cultivating and maintaining large area ECMs. Product extraction and CO_2 access to the biofilm could compromise conductivity. Engineering biofilm formation poses significant genetic engineering challenge.	Figure 7
10	Engineering a QD-DET-EMP hybrid.	No volatile intermediate (H_2). Potential for extremely low complexity system.	High complexity of genetic engineering to introduce CO_2 fixation of any sort to DET-chassis organism.	

ECM, extracellular matrix. Note that all H_2-EMP schemes have some H_2 escape and explosion hazard associated with them. The explosion risk is mitigated at laboratory scale by restricting H_2 partial pressure to 5% or less of a total of 1 atmosphere.[94] Likewise, batch culturing methods used in the lab (scenarios 1 to 3) significantly reduce the chances of H_2 escape. However, in large-scale deployment scenarios (scenarios 4 to 6) both the explosion and escape risks grow and have been noted as particular concerns. The explosion risk is significantly enhanced in scenario 6 by the use of a high-pressure atmosphere.

Alternatively, if one were to dispense with *in vivo* CO_2-fixation and replace it with *ex vivo* electrochemical CO_2 reduction and engineer *in vivo* formate assimilation (Table 2, scenario 3 or 8), efficiency gains could approach those achieved by introducing the rTCA cycle but would be much more genetically tractable. Additionally, there is room for further improvement as new artificial pathways for processing electrochemically fixed CO_2 are invented. However, this approach adds further system complexity and potential cost and would still fall short of the efficiency achieved with the incorporation of the WL pathway. Thus, the greatest gain in efficiency would require mitigating O_2-sensitivity, such as the development of O_2-tolerant versions of key enzymes or sequestering these enzymes inside O_2-impermeable cellular compartments.

The already-optimized efficiency of H_2-EMP with the Calvin cycle raises the question: is it time to take it out of the lab? And if H_2-EMP were to be optimized further with the introduction of an alternative CO_2-fixation pathway, how would such a system scale up? Agitation (Table 2, scenario 4) is the most mature, lowest cost, and most easily implemented technology for electron transport considered in this article. However, the high energy cost of stirring small volumes means that the smallest increment of storage that can be built is ≈1 MW, about the size of a large solar farm. This is very large relative to residential storage needs (the average American home uses electrical energy at the rate of about 1.3 kW) but tiny compared with the production needs for aviation fuel (when converted to jet fuel with ≈50% efficiency 1 MW corresponds to ≈50 L h^{-1}. A 787–9 consumes fuel at the rate of ≈7,000 L h^{-1}).

It is not clear that H_2-EMP will ever take on batteries for home energy storage. H_2-EMP could operate very efficiently at a small power scale if H_2 is transported by diffusion (Table 2, scenario 5). However, this approach demands a high internal area reactor. This problem can be ameliorated by operating at high H_2 pressure (Table 2, scenario 6), but it is likely that this will increase cost and incur significant safety risks. We would be foolish if we dismissed this approach outright, but we believe this analysis highlights significant technology risks. When considering real-world application, our results indicate that H_2-EMP may be best employed with agitation for very large-scale commercial applications, such as the production of jet fuel. Although one would rarely, if ever, use high-pressure H_2 in a biological laboratory setting, the use of high-pressure H_2 may not be intrinsically a problem as it is commonly used in industrial chemical processes including the Haber-Bosch process (200 to 400 MPa) and the Fischer-Tropsch process (a few 100 MPa).

Counter to intuition, the efficiency of DET-EMP using a reverse electron transport chain could almost match that of H_2-mediated EMP with laboratory overpotentials. However, at least three scientific challenges stand in the way of DET-EMP. First, as of today there is no known easily genetically engineered microbe capable of both electron uptake by DET and CO_2 fixation, meaning that this would need to be created. While the electro-cultivation method developed by Summers et al.[106] could in principle allow an electroactive microbe capable of electron uptake and CO_2-fixation like *M. ferrooxydans* PV-1 to be engineered to synthesize a biofuel, we are unaware of any report of this at the time of writing. As of today, we are still elucidating the full complement of genes encoding the reverse electron transport chain, and thus, we cannot yet estimate the complexity of the genetic engineering required to express these in an engineerable chassis organism such as *E. coli*. This question may be answered by comprehensive genomic studies of microbes thought to be capable of reverse electron transport such as *S. oneidensis*.

Second, we are unaware of any detailed models of DET-EMP reactors that incorporate conductive ECMs and CO_2-fixing electroactive microbes using a reverse electron transport chain. As a result, another open question is just how much simpler construction and operation of a DET-EMP reactor would be compared with a H_2-EMP reactor.

Finally, it is unclear how easy it would be for self-assembly of the large area ECMs that DET-EMP could rely upon. For ECMs with conductivities similar to those produced by *G. sulfurreducens* and *S. oneidensis* several square meters of ECM would

be required for every square meter of solar panel. In the lab, ECMs with areas exceeding only a few square centimeters are rarely seen.[131] If the very high reported conductivities of cable bacteria ECMs can be reproduced, these could reduce the ECM area to only a few square centimeters.

Despite these uncertainties, DET-EMP holds potential for clear advantages over H_2-EMP if these challenges can be overcome. In principle, DET-EMP coupled to a self-assembled conductive ECM could reduce construction costs; allow us to dispense with volatile intermediates like H_2, reducing safety concerns, and allow operation in an ambient atmosphere, potentially dramatically reducing operating costs as well. Furthermore, when considering real-world application, there is no obvious penalty for operating small-scale systems, meaning that DET-EMP could enable highly distributed energy storage.

We know it is possible to grow conductive ECMs with sufficiently high conductivities and thicknesses that a high-efficiency, low-footprint, relatively low internal area DET-EMP system could be produced with the microbes we already have available today. For example, while the internal areas of DET-EMP reactors using most achievable biofilm configurations, C_1 to C_3(Table 2) are between 1 and 15× the area of the solar PV supplying them, the internal area of a H_2-EMP reactor relying upon H_2 diffusion at ambient pressure will be hundreds to thousands of times the area of the PV supplying it (Figure 5). Recent developments in the construction of engineered biofilms[132] suggests that it might be possible to build a biologically synthesized conductive matrix that is tailored for EMP with low resistivity, high thickness, low area ($\leq$1× the area of the PV supplying the reactor), and high accessibility for CO_2 and product egress (Table 3, scenario 9). At the time of writing, such parameters for a biofilm are completely hypothetical, making the possibility of constructing one pure speculation, but the regular development of new cutting-edge tools for genetic engineering allows us to push the limits of what is possible. Overall, however, it remains an open question if the potential reductions in cost and system complexity of DET-EMP versus H_2-EMP are worth the trade-off in the amount of complex genetic engineering that would be needed for such a feat.

Recent developments in coupling photo-chemistry with DET[133] opens up the possibility of constructing quantum-dot (QD)-microbe hybrids that directly inject electrons in to the EET complex and then into metabolism (Table 3, scenario 10). This would allow for the development of a system free of photovoltaics and electrodes that could be deployed at potentially extremely low cost. The possibility of adjusting the redox potential of the Mtr EET complex without significantly reducing efficiency (Figure S6), along with the tunability of the electronic structure of quantum dots could allow significant room for engineering. Here, the potential for significant cost reduction could make for a significant payoff for the complex genetic engineering required to combine DET and carbon fixation.

The upper limits of efficiency of the EMP schemes presented here exceed those of all known forms of photosynthesis. Are these gains in efficiency worth pursuing? Can EMP achieve a significantly higher fraction of its theoretical efficiency in the real world than photosynthesis at an affordable cost? This analysis does not concern a specific naturally occurring or lightly engineered system but rather a highly engineered system that does not yet exist, designed to operate at the limit of its potential, so we cannot guarantee this. But, the framework developed here gives us and other investigators the ability to rapidly understand the potential bang for buck of

EMP technologies (of which there are many more than presented here), which genetic engineering interventions are worth pursuing and which are not. We hope that with the roadmap this framework gives, we and others in parallel can rapidly advance the field in multiple directions.

EXPERIMENTAL PROCEDURES

Resource Availability

Lead Contact

Further information and requests for resources and materials should be directed to and will be fulfilled by the Lead Contact, Buz Barstow (bmb35@cornell.edu).

Data and Code Availability

All computer code is available at github.com/barstowlab/rewiredcarbon.

Materials Availability

This study did not generate new unique materials.

The theory presented in this work was implemented in the REWIREDCARBON suite of software developed with Python with the SciPy[134] and NumPy[135] libraries. Initial visualization was implemented with Matplotlib[136].

SUPPLEMENTAL INFORMATION

Supplemental Information can be found online at https://doi.org/10.1016/j.joule.2020.08.010.

ACKNOWLEDGMENTS

This work was supported by a Career Award at the Scientific Interface from the Burroughs Wellcome Fund (to B.B.), Princeton University startup funds (B.B.), Cornell University startup funds (B.B.), and by US Department of Energy, Office of Biological and Environmental Research grant DE-SC0020179 (B.B.).

AUTHOR CONTRIBUTIONS

Conceptualization, B.B. and A.B.; Methodology, B.B., F.S., J.K., and R.G.; Investigation, F.S., J.K., and B.B.; Writing – Original Draft, F.S., A.M.S., and B.B.; Writing – Review & Editing, F.S., A.M.S., and B.B.; Funding Acquisition, B.B.; Resources, B.B.; Supervision, B.B. and A.B.; Data Curation, B.B. and F.S; Visualization, F.S. and B.B.; Formal Analysis, F.S., J.K., and B.B.

DECLARATION OF INTERESTS

The authors declare no competing interests.

Received: January 21, 2020
Revised: June 19, 2020
Accepted: August 17, 2020
Published: September 23, 2020

SUPPORTING CITATIONS

The following references appear in the Supplemental Information: Van Niel et al. (2002).[136–140; 143; 146–149; 151–152; 154–166; and 169]

REFERENCES

1. Huhne, C., Jones, C., Foster, A., and Ewing, F. (2011). UK renewable energy roadmap, Technical report. https://assets.publishing.service.gov.uk/government/uploads/system/uploads/attachment_data/file/48128/2167-uk-renewable-energy-roadmap.pdf.
2. MIT energy initiative (2015). The future of solar energy: an interdisciplinary MIT study, Technical report. http://energy.mit.edu/research/future-solar-energy/.
3. U.S. Energy Information Administration (2019). Annual energy outlook 2019 with projections to 2050, Technical report. https://www.eia.gov/outlooks/aeo/pdf/aeo2019.pdf.
4. Frew, B.A., Becker, S., Dvorak, M.J., Andresen, G.B., and Jacobson, M.Z. (2016). Flexibility mechanisms and pathways to a highly renewable US electricity future. Energy *101*, 65–78.
5. Shaner, M.R., Davis, S.J., Lewis, N.S., and Caldeira, K. (2018). Geophysical constraints on the reliability of solar and wind power in the United States. Energy Environ. Sci. *11*, 914–925.
6. Cebulla, F., Haas, J., Eichman, J., Nowak, W., and Mancarella, P. (2018). How much electrical energy storage do we need? A synthesis for the U.S. Europe, and Germany. J. Cleaner Prod. *181*, 449–459.
7. Salimijazi, F., Parra, E., and Barstow, B. (2019). Electrical energy storage with engineered biological systems. J. Biol. Eng. *13*, 38.
8. Herzog, H.J. (2018). Carbon Capture (MIT Press).
9. National Academies of Sciences, Engineering, and Medicine (2019). Committee on developing a research agenda for carbon dioxide removal and reliable sequestration. negative emissions technologies and reliable sequestration: a research agenda, Technical report. https://www.nap.edu/initiative/committee-on-developing-a-research-agenda-for-carbon-dioxide-removal-and-reliable-sequestration.
10. Rabaey, K., and Rozendal, R.A. (2010). Microbial electrosynthesis - revisiting the electrical route for microbial production. Nat. Rev. Microbiol. *8*, 706–716.
11. Rabaey, K., Girguis, P., and Nielsen, L.K. (2011). Metabolic and practical considerations on microbial electrosynthesis. Curr. Opin. Biotechnol. *22*, 371–377.
12. Lips, D., Schuurmans, J.M., Branco Dos Santos, F., and Hellingwerf, K.J. (2018). Many ways towards 'solar fuel': quantitative analysis of the most promising strategies and the main challenges during scale-up. Energy Environ. Sci. *11*, 10–22.
13. Claassens, N.J., Cotton, C.A.R., Kopljar, D., and Bar-Even, A. (2019). Making quantitative sense of electromicrobial production. Nat. Cat. *2*, 437–447.
14. Prévoteau, A., Carvajal-Arroyo, J.M., Ganigué, R., and Rabaey, K. (2020). Microbial electrosynthesis from CO_2: forever a promise? Curr. Opin. Biotechnol. *62*, 48–57.
15. Schröder, U., Harnisch, F., and Angenent, L.T. (2015). Microbial electrochemistry and technology: terminology and classification. Energy Environ. Sci. *8*, 513–519.
16. Yates, M.D., Eddie, B.J., Kotloski, N.J., Lebedev, N., Malanoski, A.P., Lin, B., Strycharz-Glaven, S.M., and Tender, L.M. (2016). Toward understanding long-distance extracellular electron transport in an electroautotrophic microbial community. Energy Environ. Sci. *9*, 3544–3558.
17. Korth, B., and Harnisch, F. (2019). Modeling microbial electrosynthesis. Adv. Biochem. Eng. Biotechnol. *167*, 273–325.
18. Blanchet, E., Duquenne, F., Rafrafi, Y., Etcheverry, L., Erable, B., and Bergel, A. (2015). Importance of the hydrogen route in up-scaling electrosynthesis for microbial CO 2 reduction. Energy Environ. Sci. *8*, 3731–3744.
19. Jourdin, L., Lu, Y., Flexer, V., Keller, J., and Freguia, S. (2016). Biologically induced hydrogen production drives high rate/high efficiency microbial electrosynthesis of acetate from carbon dioxide. ChemElectroChem *3*, 581–591.
20. Jiang, Y., May, H.D., Lu, L., Liang, P., Huang, X., and Ren, Z.J. (2019). Carbon dioxide and organic waste valorization by microbial electrosynthesis and electro-fermentation. Water Res *149*, 42–55.
21. Kracke, F., Wong, A.B., Maegaard, K., Deutzmann, J.S., Hubert, M.A., Hahn, C., Jaramillo, T.F., and Spormann, A.M. (2019). Robust and biocompatible catalysts for efficient hydrogen-driven microbial electrosynthesis. Commun. Chem. *2*, 45.
22. Li, H., Opgenorth, P.H., Wernick, D.G., Rogers, S., Wu, T.Y., Higashide, W., Malati, P., Huo, Y.X., Cho, K.M., and Liao, J.C. (2012). Integrated electromicrobial conversion of $CO_2$to higher alcohols. Science *335*, 1596.
23. Torella, J.P., Gagliardi, C.J., Chen, J.S., Bediako, D.K., Colón, B., Way, J.C., Silver, P.A., and Nocera, D.G. (2015). Efficient solar-to-fuels production from a hybrid microbial-water-splitting catalyst system. Proc. Natl. Acad. Sci. USA *112*, 2337–2342.
24. Liu, C., Colón, B.C., Ziesack, M., Silver, P.A., and Nocera, D.G. (2016). Water splitting-biosynthetic system with CO_2 reduction efficiencies exceeding photosynthesis. Science *352*, 1210–1213.
25. Haas, T., Krause, R., Weber, R., Demler, M., and Schmid, G. (2018). Technical photosynthesis involving CO_2 electrolysis and fermentation. Nat. Cat. *1*, 32–39.
26. Guan, J., Berlinger, S.A., Li, X., Chao, Z., Sousa E Silva, V., Banta, S., et al. (2017). Development of reactor configurations for an electrofuels platform utilizing genetically modified iron oxidizing bacteria for the reduction of CO_2 to biochemicals. J. Biotechnol. *245*, 21–27.
27. Khunjar, W.O., Sahin, A., West, A.C., Chandran, K., and Banta, S. (2012). Biomass production from electricity using ammonia as an electron carrier in a reverse microbial fuel cell. PLoS One *7*, e44846.
28. Yishai, O., Goldbach, L., Tenenboim, H., Lindner, S.N., and Bar-Even, A. (2017). Engineered assimilation of exogenous and endogenous formate in Escherichia coli. ACS Synth. Biol. *6*, 1722–1731.
29. Gleizer, S., Ben-Nissan, R., Bar-On, Y.M., Antonovsky, N., Noor, E., Zohar, Y., Jona, G., Krieger, E., Shamshoum, M., Bar-Even, A., and Milo, R. (2019). Conversion of *Escherichia coli* to generate all biomass carbon from CO2. Cell *179*, 1255–1263.e12.
30. Kim, S., Lindner, S.N., Aslan, S., Yishai, O., Wenk, S., Schann, K., and Bar-Even, A. (2020). Growth of E. coli on formate and methanol via the reductive glycine pathway. Nat. Chem. Biol. *16*, 538–545.
31. Nevin, K.P., Woodard, T.L., Franks, A.E., Summers, Z.M., and Lovley, D.R. (2010). Microbial electrosynthesis: feeding microbes electricity to convert carbon dioxide and water to multicarbon extracellular organic compounds. mBio *1*, e00103–e00110.
32. Nie, H., Zhang, T., Cui, M., Lu, H., Lovley, D.R., and Russell, T.P. (2013). Improved cathode for high efficient microbial-catalyzed reduction in microbial electrosynthesis cells. Phys. Chem. Chem. Phys. *15*, 14290–14294.
33. Su, M., Jiang, Y., and Li, D. (2013). Production of acetate from carbon dioxide in bioelectrochemical systems based on autotrophic mixed culture. J. Microbiol. Biotechnol. *23*, 1140–1146.
34. Zhang, T., Nie, H., Bain, T.S., Lu, H., Cui, M., Snoeyenbos-West, O.L., Franks, A.E., Nevin, K.P., Russell, T.P., and Lovley, D.R. (2013). Improved cathode materials for microbial electrosynthesis. Energy Environ. Sci. *6*, 217–224.
35. Marshall, C.W., Ross, D.E., Fichot, E.B., Norman, R.S., and May, H.D. (2013). Long-term operation of microbial electrosynthesis systems improves acetate production by autotrophic microbiomes. Environ. Sci. Technol. *47*, 6023–6029.
36. Jourdin, L., Freguia, S., Donose, B.C., Chen, J., Wallace, G.G., Keller, J., and Flexer, V. (2014). A novel carbon nanotube modified scaffold as an efficient biocathode material for improved microbial electrosynthesis. J. Mater. Chem. A *2*, 13093–13102.
37. LaBelle, E.V., Marshall, C.W., Gilbert, J.A., and May, H.D. (2014). Influence of acidic pH on hydrogen and acetate production by an electrosynthetic microbiome. PLoS One *9*, e109935.
38. Jourdin, L., Grieger, T., Monetti, J., Flexer, V., Freguia, S., Lu, Y., Chen, J., Romano, M., Wallace, G.G., and Keller, J. (2015). High acetic acid production rate obtained by microbial electrosynthesis from carbon dioxide. Environ. Sci. Technol. *49*, 13566–13574.
39. Bajracharya, S., Ter Heijne, A., Dominguez Benetton, X., Vanbroekhoven, K., Buisman, C.J., Strik, D.P., and Pant, D. (2015). Carbon

dioxide reduction by mixed and pure cultures in microbial electrosynthesis using an assembly of graphite felt and stainless steel as a cathode. Bioresour. Technol. *195*, 14–24.

40. Gildemyn, S., Verbeeck, K., Slabbinck, R., Andersen, S.J., Prévoteau, A., and Rabaey, K. (2015). Integrated production, extraction, and concentration of acetic acid from CO2 through microbial electrosynthesis. Environ. Sci. Technol. Lett. *2*, 325–328.

41. Patil, S.A., Arends, J.B., Vanwonterghem, I., Van Meerbergen, J., Guo, K., Tyson, G.W., and Rabaey, K. (2015). Selective enrichment establishes a stable performing community for microbial electrosynthesis of acetate from CO_2. Environ. Sci. Technol. *49*, 8833–8843.

42. Tremblay, P.L., Höglund, D., Koza, A., Bonde, I., and Zhang, T. (2015). Adaptation of the autotrophic acetogen Sporomusa ovata to methanol accelerates the conversion of CO2 to organic products. Sci. Rep. *5*, 16168.

43. Ganigué, R., Puig, S., Batlle-Vilanova, P., Balaguer, M.D., and Colprim, J. (2015). Microbial electrosynthesis of butyrate from carbon dioxide. Chem. Commun. (Camb.) *51*, 3235–3238.

44. LaBelle, E.V., and May, H.D. (2017). Energy efficiency and productivity enhancement of microbial electrosynthesis of acetate. Front. Microbiol. *8*, 756.

45. Verbeeck, K., Gildemyn, S., and Rabaey, K. (2018). Membrane electrolysis assisted gas fermentation for enhanced acetic acid production. Front. Energy Res. *6*, 88.

46. Bajracharya, S., Yuliasni, R., Vanbroekhoven, K., Buisman, C.J., Strik, D.P., and Pant, D. (2017). Long-term operation of microbial electrosynthesis cell reducing CO2 to multi-carbon chemicals with a mixed culture avoiding methanogenesis. Bioelectrochemistry *113*, 26–34.

47. Batlle-Vilanova, P., Ganigué, R., Ramió-Pujol, S., Bañeras, L., Jiménez, G., Hidalgo, M., Balaguer, M.D., Colprim, J., and Puig, S. (2017). Microbial electrosynthesis of butyrate from carbon dioxide: production and extraction. Bioelectrochemistry *117*, 57–64.

48. Raes, S.M.T., Jourdin, L., Buisman, C.J.N., and Strik, D.P.B.T.B. (2017). Continuous long-term bioelectrochemical chain elongation to butyrate. ChemElectroChem *4*, 386–395.

49. Jourdin, L., Raes, S.M., Buisman, C.J., and Strik, D.P. (2018). Critical biofilm growth throughout unmodified carbon felts allows continuous bioelectrochemical chain elongation from CO2 up to caproate at high current density. Front. Energy Res. *6*, 7.

50. del Pilar Anzola Rojas, M., Mateos, R., Sotres, A., Zaiat, M., Gonzalez, E.R., Escapa, A., De Wever, H., and Pant, D. (2018). Microbial electrosynthesis (MES) from CO2 is resilient to fluctuations in renewable energy supply. Energy Convers. Manag. *177*, 272–279.

51. Vassilev, I., Hernandez, P.A., Batlle-Vilanova, P., Freguia, S., Krömer, J.O., Keller, J., Ledezma, P., and Virdis, B. (2018). Microbial electrosynthesis of isobutyric, butyric, caproic acids, and corresponding alcohols from carbon dioxide. ACS Sustainable Chem. Eng. *6*, 8485–8493.

52. Vassilev, I., Kracke, F., Freguia, S., Keller, J., Krömer, J.O., Ledezma, P., and Virdis, B. (2019). Microbial electrosynthesis system with dual biocathode arrangement for simultaneous acetogenesis, solventogenesis and carbon chain elongation. Chem. Commun. (Camb.) *55*, 4351–4354.

53. Zhu, X.G., Long, S.P., and Ort, D.R. (2008). What is the maximum efficiency with which photosynthesis can convert solar energy into biomass? Curr. Opin. Biotechnol. *19*, 153–159.

54. Zhu, X.G., Long, S.P., and Ort, D.R. (2010). Improving photosynthetic efficiency for greater yield. Annu. Rev. Plant Biol. *61*, 235–261.

55. Green, M.A., Hishikawa, Y., Dunlop, E.D., Levi, D.H., Hohl-Ebinger, J., Yoshita, M., and Ho-Baillie, A.W. (2019). Solar cell efficiency tables, (version 53). Prog. Photovolt Res. Appl. *27*, 3–12.

56. Wijffels, R.H., and Barbosa, M.J. (2010). An outlook on microalgal biofuels. Science *329*, 796–799.

57. Tashiro, Y., Hirano, S., Matson, M.M., Atsumi, S., and Kondo, A. (2018). Electrical-biological hybrid system for CO_2 reduction. Metab. Eng. *47*, 211–218.

58. Lu, X., Withers, M.R., Seifkar, N., Field, R.P., Barrett, S.R., and Herzog, H.J. (2015). Biomass logistics analysis for large scale biofuel production: case study of loblolly pine and switchgrass. Bioresour. Technol. *183*, 1–9.

59. Adesina, O., Anzai, I.A., Avalos, J.L., and Barstow, B. (2017). Embracing biological solutions to the sustainable energy challenge. Chem *2*, 20–51.

60. Köpke, M., Mihalcea, C., Bromley, J.C., and Simpson, S.D. (2011). Fermentative production of ethanol from carbon monoxide. Curr. Opin. Biotechnol. *22*, 320–325.

61. Yu, J. (2014). Bio-based products from solar energy and carbon dioxide. Trends Biotechnol *32*, 5–10.

62. Barstow, B. (2015). Molecular mechanisms for the biological storage of renewable energy. Adv. Sci. Eng. Med. *7*, 1066–1081.

63. Glaven, S.M. (2019). Bioelectrochemical systems and synthetic biology: more power, more products. Microb. Biotechnol. *12*, 819–823.

64. Shockley, W., and Queisser, H.J. (1961). Detailed balance limit of efficiency of p-n junction solar cells. J. Appl. Phys. *32*, 510–519.

65. Vos, A.D. (1980). Detailed balance limit of the efficiency of tandem solar cells. J. Phys. D Appl. Phys. *13*, 839–846.

66. Nelson, J. (2003). The Physics of Solar Cells (Imperial College Press).

67. Korth, B., Rosa, L.F., Harnisch, F., and Picioreanu, C. (2015). A framework for modeling electroactive microbial biofilms performing direct electron transfer. Bioelectrochemistry *106*, 194–206.

68. Pandit, A.V., and Mahadevan, R. (2011). In silico characterization of microbial electrosynthesis for metabolic engineering of biochemicals. Microb. Cell Fact. *10*, 76.

69. Kazemi, M., Biria, D., and Rismani-Yazdi, H. (2015). Modelling bio-electrosynthesis in a reverse microbial fuel cell to produce acetate from CO2 and H2O. Phys. Chem. Chem. Phys. *17*, 12561–12574.

70. Grousseau, E., Lu, J., Gorret, N., Guillouet, S.E., and Sinskey, A.J. (2014). Isopropanol production with engineered *Cupriavidus necator* as bioproduction platform. Appl. Microbiol. Biotechnol. *98*, 4277–4290.

71. Lu, J., Brigham, C.J., Gai, C.S., and Sinskey, A.J. (2012). Studies on the production of branched-chain alcohols in engineered *Ralstonia eutropha*. Appl. Microbiol. Biotechnol. *96*, 283–297.

72. Ueki, T., Nevin, K.P., Woodard, T.L., Aklujkar, M.A., Holmes, D.E., and Lovley, D.R. (2018). Construction of a *Geobacter* strain With exceptional growth on cathodes. Front. Microbiol. *9*, 1512.

73. Appel, A.M., Bercaw, J.E., Bocarsly, A.B., Dobbek, H., Dubois, D.L., Dupuis, M., Ferry, J.G., Fujita, E., Hille, R., Kenis, P.J., et al. (2013). Frontiers, opportunities, and challenges in biochemical and chemical catalysis of CO_2 fixation. Chem. Rev. *113*, 6621–6658.

74. White, J.L., Herb, J.T., Kaczur, J.J., Majsztrik, P.W., and Bocarsly, A.B. (2014). Photons to formate: efficient electrochemical solar energy conversion via reduction of carbon dioxide. J. CO2 Util. *7*, 1–5.

75. White, J.L., Baruch, M.F., Pander, J.E., Iii, Hu, Y., Fortmeyer, I.C., Park, J.E., Zhang, T., Liao, K., Gu, J., Yan, Y., et al. (2015). Light-driven heterogeneous reduction of carbon dioxide: photocatalysts and photoelectrodes. Chem. Rev. *115*, 12888–12935.

76. Burgdorf, T., Lenz, O., Buhrke, T., van der Linden, E., Jones, A.K., Albracht, S.P., et al. (2005). [NiFe]-hydrogenases of *Ralstonia eutropha* H16: modular enzymes for oxygen-tolerant biological hydrogen oxidation. J. Mol. Microbiol. Biotechnol. *10*, 181–196.

77. Agapakis, C.M., Ducat, D.C., Boyle, P.M., Wintermute, E.H., Way, J.C., and Silver, P.A. (2010). Insulation of a synthetic hydrogen metabolism circuit in bacteria. J. Biol. Eng. *4*, 3.

78. Barstow, B., Agapakis, C.M., Boyle, P.M., Grandl, G., Silver, P.A., and Wintermute, E.H. (2011). A synthetic system links FeFe-hydrogenases to essential *E. coli* sulfur metabolism. J. Biol. Eng. *5*, 7.

79. Ducat, D.C., Sachdeva, G., and Silver, P.A. (2011). Rewiring hydrogenase-dependent redox circuits in cyanobacteria. Proc. Natl. Acad. Sci. USA *108*, 3941–3946.

80. Huber, H., Gallenberger, M., Jahn, U., Eylert, E., Berg, I.A., Kockelkorn, D., Eisenreich, W., and Fuchs, G. (2008). A dicarboxylate/4-hydroxybutyrate autotrophic carbon assimilation cycle in the hyperthermophilic *Archaeum ignicoccus hospitalis*. Proc. Natl. Acad. Sci. USA *105*, 7851–7856.

81. Berlin, N.I., Waldmann, T.A., and Weissman, S.M. (1959). Life span of red blood cell. Physiol. Rev. *39*, 577–616.

82. Kliphuis, A.M.J., Klok, A.J., Martens, D.E., Lamers, P.P., Janssen, M., and Wijffels, R.H. (2012). Metabolic modeling of *Chlamydomonas reinhardtii*: energy requirements for photoautotrophic growth and maintenance. J. Appl. Phycol. *24*, 253–266.

83. Schwander, T., Schada von Borzyskowski, L.S., Burgener, S., Cortina, N.S., and Erb, T.J. (2016). A synthetic pathway for the fixation of carbon dioxide *in vitro*. Science *354*, 900–904.

84. Milo, R., Jorgensen, P., Moran, U., Weber, G., and Springer, M. (2010). BioNumbers - the database of key numbers in molecular and cell biology. Nucleic Acids Res. *38*, D750–D753.

85. Chernet, B.T., and Levin, M. (2013). Transmembrane voltage potential is an essential cellular parameter for the detection and control of tumor development in a Xenopus model. Dis. Models Mech. *6*, 595–607.

86. Van Walraven, H.S., Strotmann, H., Schwarz, O., and Rumberg, B. (1996). The H^+/ATP coupling ratio of the ATP synthase from thiol-modulated chloroplasts and two cyanobacterial strains is four. FEBS Lett. *379*, 309–313.

87. Schink, B. (1997). Energetics of syntrophic cooperation in methanogenic degradation. Microbiol. Mol. Biol. Rev. *61*, 262–280.

88. Esswein, A.J., Surendranath, Y., Reece, S.Y., and Nocera, D.G. (2011). Highly active cobalt phosphate and borate based oxygen evolving catalysts operating in neutral and natural waters. Energy Environ. Sci. *4*, 499–504.

89. Marshall, C.W., Ross, D.E., Handley, K.M., Weisenhorn, P.B., Edirisinghe, J.N., Henry, C.S., Gilbert, J.A., May, H.D., and Norman, R.S. (2017). Metabolic reconstruction and modeling microbial electrosynthesis. Sci. Rep. *7*, 8391.

90. Bothe, H., Schmitz, O., Yates, M.G., and Newton, W.E. (2010). Nitrogen fixation and hydrogen metabolism in cyanobacteria. Microbiol. Mol. Biol. Rev. *74*, 529–551.

91. Chen, A.H., Robinson-Mosher, A., Savage, D.F., Silver, P.A., and Polka, J.K. (2013). The bacterial carbon-fixing organelle is formed by shell envelopment of preassembled cargo. PLoS One *8*, e76127.

92. Polka, J.K., and Silver, P.A. (2016). A tunable protein piston that breaks membranes to release encapsulated cargo. ACS Synth. Biol. *5*, 303–311.

93. Butterfield, G.L., Lajoie, M.J., Gustafson, H.H., Sellers, D.L., Nattermann, U., Ellis, D., Bale, J.B., Ke, S., Lenz, G.H., Yehdego, A., et al. (2017). Evolution of a designed protein assembly encapsulating its own RNA genome. Nature *552*, 415–420.

94. Brigham, C.J., Gai, C.S., Lu, J., Speth, D.R., Worden, R.M., and Sinskey, A.J. (2013). Engineering *Ralstonia eutropha* for production of isobutanol from CO_2, H_2, and O_2. In Advanced Biofuels and Bioproducts, J.W. Lee, ed. (Springer), pp. 1065–1090.

95. Tanaka, K., Ishizaki, A., Kanamaru, T., and Kawano, T. (1995). Production of poly(D-3-hydroxybutyrate) from CO_2, H_2, and O_2 by high cell density autotrophic cultivation of *Alcaligenes eutrophus*. Biotechnol. Bioeng. *45*, 268–275.

96. Worden, R.M., and Liu, Y.C. (2014) Catalytic bioreactors and methods of using same. US Patents US20140187826A1, Filed, 6 March, 2014, Published, July 3, 2014.

97. Van't Riet, K. (1979). Review of measuring methods and results in nonviscous gas-liquid mass transfer in stirred vessels. Ind. Eng. Chem. Proc. Des. Dev. *18*, 357–364.

98. Sydow, A., Krieg, T., Mayer, F., Schrader, J., and Holtmann, D. (2014). Electroactive bacteria–molecular mechanisms and genetic tools. Appl. Microbiol. Biotechnol. *98*, 8481–8495.

99. Fredrickson, J.K., Romine, M.F., Beliaev, A.S., Auchtung, J.M., Driscoll, M.E., Gardner, T.S., Nealson, K.H., Osterman, A.L., Pinchuk, G., Reed, J.L., et al. (2008). Towards environmental systems biology of *Shewanella*. Nat. Rev. Microbiol. *6*, 592–603.

100. Shi, L., Rosso, K.M., Clarke, T.A., Richardson, D.J., Zachara, J.M., and Fredrickson, J.K. (2012). Molecular underpinnings of Fe(III) oxide reduction by *Shewanella oneidensis* MR-1. Front. Microbiol. *3*, 50.

101. Shi, L., Dong, H., Reguera, G., Beyenal, H., Lu, A., Liu, J., Yu, H.Q., and Fredrickson, J.K. (2016). Extracellular electron transfer mechanisms between microorganisms and minerals. Nat. Rev. Microbiol. *14*, 651–662.

102. Bird, L.J., Bonnefoy, V., and Newman, D.K. (2011). Bioenergetic challenges of microbial iron metabolisms. Trends Microbiol. *19*, 330–340.

103. Thauer, R.K., Jungermann, K., and Decker, K. (1977). Energy conservation in chemotrophic anaerobic bacteria. Bacteriol. Rev. *41*, 100–180.

104. Liu, J., Wang, Z., Belchik, S.M., Edwards, M.J., Liu, C., Kennedy, D.W., Merkley, E.D., Lipton, M.S., Butt, J.N., Richardson, D.J., et al. (2012). Identification and characterization of MtoA: a decaheme c-type cytochrome of the neutrophilic Fe(II)-oxidizing bacterium *Sideroxydans lithotrophicus* ES-1. Front. Microbiol. *3*, 1–11.

105. Bonis, B.M., and Gralnick, J.A. (2015). *Marinobacter subterrani*, a genetically tractable neutrophilic Fe(II)- oxidizing strain isolated from the Soudan iron mine. Front. Microbiol. *6*, 719.

106. Summers, Z.M., Gralnick, J.A., and Bond, D.R. (2013). Cultivation of an obligate Fe(II)-oxidizing lithoautotrophic bacterium using electrodes. mBio *4*, e00412–e00420.

107. Canfield, D.E., Rosing, M.T., and Bjerrum, C. (2006). Early anaerobic metabolisms. Philos. Trans. R. Soc. Lond. B Biol. Sci. *361*, 1819–1834, discussion 1835.

108. Rowe, A.R., Rajeev, P., Jain, A., Pirbadian, S., Okamoto, A., Gralnick, J.A., El-Naggar, M.Y., and Nealson, K.H. (2018). Tracking electron uptake from a cathode into *Shewanella* cells: implications for energy acquisition from solid-substrate electron donors. mBio *9*, 1–19.

109. Bose, A., Gardel, E.J., Vidoudez, C., Parra, E.A., and Girguis, P.R. (2014). Electron uptake by iron-oxidizing phototrophic bacteria. Nat. Commun. *5*, 3391.

110. Tang, H.Y., Holmes, D.E., Ueki, T., Palacios, P.A., and Lovley, D.R. (2019). Iron corrosion via direct metal-microbe electron transfer. mBio *10*, 1–10.

111. Zheng, Z., Xiao, Y., Wu, R., Mølager Christensen, H.E., Zhao, F., and Zhang, J. (2019). Electrons selective uptake of a metal-reducing bacterium *Shewanella oneidensis* MR-1 from ferrocyanide. Biosens. Bioelectron. *142*, 111571.

112. Hoijnen, J.J., van Loosdrecht, M.C., and Tijhuis, L. (1992). A black box mathematical model to calculate auto- and heterotrophic biomass yields based on Gibbs energy dissipation. Biotechnol. Bioeng. *40*, 1139–1154.

113. Firer-Sherwood, M., Pulcu, G.S., and Elliott, S.J. (2008). Electrochemical interrogations of the Mtr cytochromes from *Shewanella*: opening a potential window. J. Biol. Inorg. Chem. *13*, 849–854.

114. Chadwick, G.L., Jiménez Otero, F.J., Gralnick, J.A., Bond, D.R., and Orphan, V.J. (2019). NanoSIMS imaging reveals metabolic stratification within current-producing biofilms. Proc. Natl. Acad. Sci. USA *116*, 20716–20724.

115. Snider, R.M., Strycharz-Glaven, S.M., Tsoi, S.D., Erickson, J.S., and Tender, L.M. (2012). Long-range electron transport in *Geobacter sulfurreducens* biofilms is redox gradient-driven. Proc. Natl. Acad. Sci. USA *109*, 15467–15472.

116. Yates, M.D., Golden, J.P., Roy, J., Strycharz-Glaven, S.M., Tsoi, S., Erickson, J.S., El-Naggar, M.Y., Calabrese Barton, S.C., and Tender, L.M. (2015). Thermally activated long range electron transport in living biofilms. Phys. Chem. Chem. Phys. *17*, 32564–32570.

117. Zacharoff, L.A., and El-Naggar, M.Y. (2017). Redox conduction in biofilms: from respiration to living electronics. Curr. Opin. Electrochem. *4*, 182–189.

118. Yates, M.D., Barr Engel, S.B., Eddie, B.J., Lebedev, N., Malanoski, A.P., and Tender, L.M. (2018). Redox-gradient driven electron transport in a mixed community anodic biofilm. FEMS Microbiol. Ecol. *94*.

119. Wang, F., Gu, Y., O'Brien, J.P., Yi, S.M., Yalcin, S.E., Srikanth, V., Shen, C., Vu, D., Ing, N.L., Hochbaum, A.I., et al. (2019). Structure of microbial nanowires reveals stacked hemes that transport electrons over micrometers. Cell *177*, 361–369.e10.

120. Ing, N.L., Nusca, T.D., and Hochbaum, A.I. (2017). *Geobacter sulfurreducens* pili support ohmic electronic conduction in aqueous solution. Phys. Chem. Chem. Phys. *19*, 21791–21799.

121. Malvankar, N.S., Tuominen, M.T., and Lovley, D.R. (2012). Biofilm conductivity is a decisive variable for high-current-density *Geobacter*

sulfurreducens microbial fuel cells. Energy Environ. Sci. *5*, 5790–5797.

122. Renslow, R., Babauta, J., Kuprat, A., Schenk, J., Ivory, C., Fredrickson, J., and Beyenal, H. (2015). Mathematical modeling of extracellular electron transfer in biofilms. In Biofilms in Bioelectrochemical Systems, H. Beyenal and J. Babauta, eds. (John Wiley & Sons, Ltd), pp. 281–344.

123. El-Naggar, M.Y., Wanger, G., Leung, K.M., Yuzvinsky, T.D., Southam, G., Yang, J., Lau, W.M., Nealson, K.H., and Gorby, Y.A. (2010). Electrical transport along bacterial nanowires from *Shewanella oneidensis* MR-1. Proc. Natl. Acad. Sci. USA *107*, 18127–18131.

124. Meysman, F.J.R., Cornelissen, R., Trashin, S., Bonné, R., Martinez, S.H., van der Veen, J., Blom, C.J., Karman, C., Hou, J.L., Eachambadi, R.T., et al. (2019). A highly conductive fibre network enables centimetre-scale electron transport in multicellular cable bacteria. Nat. Commun. *10*, 4120.

125. Pfeffer, C., Larsen, S., Song, J., Dong, M., Besenbacher, F., Meyer, R.L., Kjeldsen, K.U., Schreiber, L., Gorby, Y.A., El-Naggar, M.Y., et al. (2012). Filamentous bacteria transport electrons over centimetre distances. Nature *491*, 218–221.

126. Kang, H.C., and Geckeler, K.E. (2000). Enhanced electrical conductivity of polypyrrole prepared by chemical oxidative polymerization: effect of the preparation technique and polymer additive. Polymer *41*, 6931–6934.

127. Yu, Y.Y., Chen, H.L., Yong, Y.C., Kim, D.H., and Song, H. (2011). Conductive artificial biofilm dramatically enhances bioelectricity production in *Shewanella* -inoculated microbial fuel cells. Chem. Commun. (Camb.) *47*, 12825–12827.

128. Siegel, J.B., Smith, A.L., Poust, S., Wargacki, A.J., Bar-Even, A., Louw, C., Shen, B.W., Eiben, C.B., Tran, H.M., Noor, E., et al. (2015). Computational protein design enables a novel one-carbon assimilation pathway. Proc. Nat. Acad. Sci. U S A *112*, 3704–3709.

129. Bar-Even, A. (2016). Formate assimilation: the metabolic architecture of natural and synthetic pathways. Biochemistry *55*, 3851–3863.

130. Antonovsky, N., Gleizer, S., Noor, E., Zohar, Y., Herz, E., Barenholz, U., Zelcbuch, L., Amram, S., Wides, A., Tepper, N., et al. (2016). Sugar synthesis from CO2 in Escherichia coli. Cell *166*, 115–125.

131. Beyenal, H., and Babauta, J. (2015). Biofilms in Bioelectrochemical Systems (John Wiley & Sons).

132. Nguyen, P.Q., Botyanszki, Z., Tay, P.K.R., and Joshi, N.S. (2014). Programmable biofilm-based materials from engineered curli nanofibres. Nat. Commun. *5*, 4945.

133. Rowe, S.F., Gall, G.L., Ainsworth, E.V., Davies, J.A., Lockwood, C.W.J., Shi, L., Elliston, A., Roberts, I.N., Waldron, K.W., Richardson, D.J., et al. (2017). Light-driven H_2-evolution and C=C or C=O Bond hydrogenation by *Shewanella oneidensis*: a versatile strategy for photocatalysis by nonphotosynthetic microorganisms. ACS Catal. *7*, 7558–7566.

134. Virtanen, P., Gommers, R., Oliphant, T.E., Haberland, M., Reddy, T., Cournapeau, D., Burovski, E., Peterson, P., Weckesser, W., Bright, J., et al. (2019). SciPy 1.0–fundamental algorithms for scientific computing in Python. arXiv. https://arxiv.org/abs/1907.10121.

135. van der Walt, S., Colbert, S.C., and Varoquaux, G. (2010). The NumPy array: a structure for efficient numerical computation. Comput. Sci. Eng. *13*, 22–30.

136. Hunter, J.D. (2007). Matplotlib: a 2D graphics environment. Comput. Sci. Eng. *9*, 90–95.

137. Lea-Smith, D.J., Bombelli, P., Vasudevan, R., and Howe, C.J. (2016). Photosynthetic, respiratory and extracellular electron transport pathways in cyanobacteria. Biochim. Biophys. Acta Bioenerg. *1857*, 247–255.

138. Bird, R.E., Hulstrom, R.L., and Lewis, L.J. (1983). Terrestrial solar spectral data sets. Sol. Energy *30*, 563–573.

139. The National Renewable Energy Laboratory Reference Air Mass 1.5 Spectra. https://www.nrel.gov/grid/solar-resource/spectra-am1.5.html.

140. Noggle, J.H. (1996). Physical Chemistry (Harper Collins).

141. Jannasch, H.W., Wirsen, C.O., and Doherty, K.W. (1996). A pressurized chemostat for the study of marine barophilic and oligotrophic bacteria. Appl. Environ. Microbiol. *62*, 1593–1596.

142. Vanniel, E.W., Budde, M.A., De Haas, G., Van der Wal, F.J., Claassen, P.A., and Stams, A.J. (2002). Distinctive properties of high hydrogen producing extreme thermophiles, Caldicellulosiruptor saccharolyticus and Thermotoga elfii. Int. J. Hydr. Energy *27*, 1391–1398.

143. Ibrahim, M.H., and Steinbüchel, A. (2010). High-cell-density cyclic fed-batch fermentation of a poly(3- hydroxybutyrate)-accumulating thermophile, *Chelatococcus* sp. strain MW10. Appl. Environ. Microbiol. *76*, 7890–7895.

144. Godfroy, A., Raven, N.D., and Sharp, R.J. (2000). Physiology and continuous culture of the hyperthermophilic deep-sea vent archaeon *Pyrococcus abyssi* ST549. FEMS Microbiol. Lett. *186*, 127–132.

145. Lippi, L., Bähr, L., Wüstenberg, A., Wilde, A., and Steuer, R. (2018). Exploring the potential of high-density cultivation of cyanobacteria for the production of cyanophycin. Algal Res *31*, 363–366.

146. Cammack, R., Rao, K.K., Bargeron, C.P., Hutson, K.G., Andrew, P.W., and Rogers, L.J. (1977). Midpoint redox potentials of plant and algal ferredoxins. Biochem. J. *168*, 205–209.

147. Schoepp-Cothenet, B., Lieutaud, C., Baymann, F., Verméglio, A., Friedrich, T., Kramer, D.M., and Nitschke, W. (2009). Menaquinone as pool quinone in a purple bacterium. Proc. Natl. Acad. Sci. USA *106*, 8549–8554.

148. Wagner, G.C., Kassner, R.J., and Kamen, M.D. (1974). Redox potentials of certain vitamins K: implications for a role in sulfite reduction by obligately anaerobic bacteria. Proc. Natl. Acad. Sci. USA *71*, 253–256.

149. Speers, A.M., and Reguera, G. (2015). Theoretical and practical considerations for culturing *Geobacter* biofilms in microbial fuel cells and other bioelectrochemical systems. In Biofilms in Bioelectrochemical Systems, H. Beyenal and J. Babauta, eds. (John Wiley & Sons, Ltd), pp. 37–59.

150. Malvankar, N.S., and Lovley, D.R. (2015). Electronic conductivity in living biofilms: physical meaning, mechanisms, and measurement methods. In Biofilms in Bioelectrochemical Systems, H. Beyenal and J. Babauta, eds. (John Wiley & Sons, Ltd), pp. 211–248.

151. Renslow, R.S., Majors, P.D., McLean, J.S., Fredrickson, J.K., Ahmed, B., and Beyenal, H. (2010). *In situ* effective diffusion coefficient profiles in live biofilms using pulsed-field gradient nuclear magnetic resonance. Biotechnol. Bioeng. *106*, 928–937.

152. Hung, C., Zhou, Y., Pinkner, J.S., Dodson, K.W., Crowley, J.R., Heuser, J., Chapman, M.R., Hadjifrangiskou, M., Henderson, J.P., and Hultgren, S.J. (2013). *Escherichia coli* biofilms have an organized and complex extracellular matrix structure. mBio *4*, e00613–e00645.

153. Hammo, S.M. (2012). Effect of Acidic Dopants properties on the Electrical Conductivity of Polyaniline. Tikrit J. Pure Sci. *17*, 76–78.

154. Schomburg, I., Jeske, L., Ulbrich, M., Placzek, S., Chang, A., and Schomburg, D. (2017). The BRENDA enzyme information system-from a database to an expert system. J. Biotechnol. *261*, 194–206.

155. Shin, J., Song, Y., Jin, S., Cho, S., and Cho, B.-K. (2017). Microbial conversion of carbon dioxide to electrofuels. In Consequences of Microbial Interactions with Hydrocarbons, Oils, and Lipids: Production of Fuels and Chemicals, S.Y. Lee, ed. (Springer International Publishing), pp. 167–182.

156. Yu, H., Li, X., Duchoud, F., Chuang, D.S., and Liao, J.C. (2018). Augmenting the Calvin-Benson-Bassham cycle by a synthetic malyl-CoA-glycerate carbon fixation pathway. Nat. Commun. *9*, 2008.

157. Berg, I.A. (2011). Ecological aspects of the distribution of different autotrophic CO_2 fixation pathways. Appl. Environ. Microbiol. *77*, 1925–1936.

158. Schadeweg, V., and Boles, E. (2016). *n*-butanol production in *Saccharomyces cerevisiae* is limited by the availability of coenzyme A and cytosolic acetyl-CoA. Biotechnol. Biofuels *9*, 44.

159. Berg, J., Tymoczko, J., and Stryer, L. (2002). Biochemistry, Fifth Edition (W H Freeman).

160. Alissandratos, A., and Easton, C.J. (2015). Biocatalysis for the application of CO_2as a chemical feedstock. Beilstein J. Org. Chem. *11*, 2370–2387.

161. Claassens, N.J., Sousa, D.Z., dos Santos, V.A.M., de Vos, W.M., and van der Oost, J.

(2016). Harnessing the power of microbial autotrophy. Nat. Rev. Microbiol. *14*, 692–706.

162. Berg, I.A., Kockelkorn, D., Buckel, W., and Fuchs, G. (2007). A 3-Hydroxypropionate/4-Hydroxybutyrate autotrophic carbon dioxide assimilation pathway in Archaea. Science *318*, 1782–1786.

163. Zarzycki, J., Brecht, V., Müller, M., and Fuchs, G. (2009). Identifying the missing steps of the autotrophic 3-hydroxypropionate CO_2 fixation cycle in *Chloroflexus aurantiacus*. Proc. Natl. Acad. Sci. USA *106*, 21317–21322.

164. Herter, S., Fuchs, G., Bacher, A., and Eisenreich, W. (2002). A bicyclic autotrophic CO_2 fixation pathway in *Chloroflexus aurantiacus*. J. Biol. Chem. *277*, 20277–20283.

165. Blackstock, J.C. (1989). The tricarboxylate cycle. In Guide to Biochemistry, J.C. Blackstock, ed. (Butterworth-Heinemann), pp. 149–159.

166. Pirt, S.J. (1965). The maintenance energy of bacteria in growing cultures. Proc. R. Soc. Lond. B Biol. Sci. *163*, 224–231.

167. Zhang, W., Hu, Y., Ma, L., Zhu, G., Wang, Y., et al. (2018). Progress and Perspective of Electrocatalytic CO_2 Reduction for Renewable Carbonaceous Fuels and Chemicals. Advanced Science *5*, https://doi.org/10.1002/advs.201700275.

168. Rasul, S., Pugnant, A., Xiang, H., Fontmorin, J.-M., and Yu, E. (2019). Low cost and efficient alloy electrocatalysts for CO_2 reduction to formate. Journal of CO_2 Utilization *23*, 1–10.

169. Van Niel, E.W., et al. (2002). Distinctive properties of high hydrogen producing extreme thermophiles, *Caldicellulosiruptor saccharolyticus* and *Thermotoga elfii*. International Journal of Hydrogen Energy *27*, 1391–1398.